New Mexico Nano-Energetics, Inc.

117 Chapel Lane, Española, NM 87532
tel: (505) 753-5499 fax: (505) 753-5499

"Development of a Dynamic Gas Condensation Technique for Commercial Production of Nanometer Metal Powders: Final Report"

by
Joe A. Martin, Ph.D.

Contract Number: N68936-97-C-0040
SBIR Phase I
Date of report: May 25, 1997
Reporting period: November 6, 1996 through May 5, 1997

CDRL Data Item Number: A001 (TECHNICAL REPORT-STUDY/SERVICES)

Item Number: 0001AF (Final Report)
Shipment AAA0006

Contract amount: $69,105.96, competitively awarded.

Sponsor: Don Thompson
Code 47340D
Naval Air Warfare Center - Weapons Division
China Lake, CA 93555-6100

UNCLASSIFIED

Issuing Activity: NAVAL AIR WARFARE CENTER WEAPONS DIVISION

REPORT DOCUMENTATION PAGE

Form Approved
OMB No. 0704-0188

1. AGENCY USE ONLY *(Leave blank)*	2. REPORT DATE	3. REPORT TYPE AND DATES COVERED
	25MAY97	FINAL REPORT, 6NOV96-5MAY97

4. TITLE AND SUBTITLE
Development of a Dynamic Gas Condensation Technique for Commercial Production of Nanometer Metal Powders

5. FUNDING NUMBERS
C N68936-97-C-0040

6. AUTHOR(S)
Joe A. Martin, Ph.D.

7. PERFORMING ORGANIZATION NAME(S) AND ADDRESS(ES)
New Mexico Nano-Energetics, Inc.
117 Chapel Lane
Espanola, NM 87532

8. PERFORMING ORGANIZATION REPORT NUMBER
0001AF

9. SPONSORING/MONITORING AGENCY NAME(S) AND ADDRESS(ES)
Don Thompson, Code 473430D
Naval Air Warfare Center - Weapons Division
China Lake, CA 93555-6100

10. SPONSORING/MONITORING AGENCY REPORT NUMBER

11. SUPPLEMENTARY NOTES
None

12a. DISTRIBUTION/AVAILABILITY STATEMENT
Approved for public release; distribution is unlimited.

12b. DISTRIBUTION CODE

13. ABSTRACT *(Maximum 200 words)*

The feasibility of utilizing dynamic gas condensation technology to commercially produce nanometer-scale metal powders is determined in this project. The elements of the determination are: to design and construct a laboratory-scale apparatus to produce samples of three different nanometer-scale metal powders, to measure purity, particle size and particle size distribution of the powder samples, and to design a plan for construction of a prototype apparatus that can produce 1-2 kilograms of nanometer-scale powder per day. We describe the design and operation of a laboratory-scale apparatus based on a medium-power radio frequency induction source. Transmission electron microscopy and high-energy ion scattering measurements are presented for aluminum, magnesium and copper powders that were produced. Typical particle sizes are in the range 10-70 nanometers. Design recommendations and a plan for construction of a larger-scale apparatus is given. We conclude that the use of dynamic gas condensation to fabricate nanometer-scale metal powder is commercially feasible.

14. SUBJECT TERMS
condensation, nanometer, powder, metastable, passivation, induction, metal, composite

15. NUMBER OF PAGES
34

16. PRICE CODE

17. SECURITY CLASSIFICATION OF REPORT	18. SECURITY CLASSIFICATION OF THIS PAGE	19. SECURITY CLASSIFICATION OF ABSTRACT	20. LIMITATION OF ABSTRACT
UNCLASSIFIED	UNCLASSIFIED	UNCLASSIFIED	

NSN 7540-01-280-5500

Standard Form 298 (Rev. 2-89)
Prescribed by ANSI Std. 239-18
298-102

TABLE OF CONTENTS

The format and ordering used in this report follows that outlined in the preparation instructions section of the Data Item Description (Identification Number: DI-MISC-80508) of contract N68936-97-C-0040.

SECTION I

Introduction

The objective of this Phase I research effort is to determine the commercial feasibility of utilizing dynamic gas condensation technology to produce nanometer-scale metal powders. The essential elements of the feasibility determination are: 1) to design and construct a small apparatus to produce samples of three different nanometer-scale metal powders using dynamic gas condensation, 2) to measure purity, particle size, and particle size distribution of the powder samples that are produced, and 3) to design a plan for construction of a larger prototype apparatus that can produce 1-2 kilograms of nanometer-scale powder per day. It is expected that the resulting plan for construction will be implemented in a Phase II contract.

Executive Summary

All of the goals specified in solicitation N96-244 have been successfully achieved in this Phase I project. The work was accomplished according to the schedule and budget outlined in our Phase I proposal. We have demonstrated that the dynamic gas condensation technique is a feasible method of producing nanometer-scale metal powders that exhibit the specific physical characteristics that were requested in N96-244.

Our project approach was to construct a laboratory-scale, dynamic gas condensation apparatus and use it to determine the feasibility of the dynamic gas condensation technique for nanometer-scale metal powder production. The technique involves evaporating bulk metals into an inert gas atmosphere. Metal vapor is cooled through collisions with inert gas molecules and, when sufficiently cool, dynamically condenses to form nanometer-scale metal clusters. We demonstrated that pure and passivated powders of aluminum, magnesium, and copper can be readily produced using the technique. We produced metal powders with average particle diameters in the 10-70 nanometer range, with narrow particle size distributions. The laboratory-scale work permitted us to obtain critical design parameters that we subsequently used to formulate a design and plan for construction for a small-scale apparatus that can produce 1-2 kilograms of nanometer-scale powders per day.

Conclusions

The project has established that the dynamic gas condensation technique is feasible for commercial production of nanometer-scale metal powders. As part of our work, we constructed a laboratory-scale, dynamic gas condensation apparatus based upon a medium-power (2.5 kW), radio frequency (rf) induction source, operating near 200 kHz. From our laboratory-scale results, we conclude that rf induction heating is an efficient method of vaporizing bulk metals for the dynamic gas condensation technique. The apparatus can be scaled to larger size by using a large-scale (e.g., 200kW) rf induction

power source, to produce commercially significant production levels of nanometer-scale metal powders.

It is our conclusion that the dynamic gas condensation technique is amenable to the production of a variety of nanometer-scale metal powders. For this project, our efforts were focused on the production of three metal powders; aluminum, magnesium, and copper. However, we also briefly explored using the technique to produce titanium and tungsten powders. It is our conclusion that higher power densities are necessary than can be achieved with the 2.5 kW rf source that was used in this study to produce nanometer-scale powders of titanium and tungsten.

The aluminum, magnesium, and copper powders were analyzed for purity, particle morphology, average particle size, particle size distribution, and passivation layer characteristics using high-energy ion scattering and high-resolution transmission electron microscopy (HRTEM). Two high-energy ion scattering techniques were used to determine powder purity, Rutherford backscattering spectrometry (RBS) and a nuclear resonance scattering technique. RBS was used as the standard purity measurement technique and a nuclear resonance scattering technique was used for high-sensitivity oxygen measurements. HRTEM was used to determine particle morphology, average size, size distribution, and passivation layer characteristics. Briefly, the analytical results are summarized below:

Aluminum:

1) Particle morphology is roughly spherical, with a passivating layer.
2) Particle interiors are single-crystal aluminum.
3) Passivation layer is continuous, amorphous Al_2O_3; nominally 3 nm thick.
4) Average particle diameter is 31 nm.
5) Particle size distribution is narrow, with a full-width-at-half maximum (FWHM) of 17 nm.
6) Passivated powder is not pyrophoric and is stable to at least 400 C in air.
7) Powder is extremely pure, typically 69% Al and 31% O, with less than 0.1 atomic percent impurities.

Magnesium:

1) Particle morphology is that of a right hexagon, with a passivating layer.
2) Particle interiors are single-crystal magnesium.
3) Passivation layer is continuous, crystalline MgO; nominally 2.5 nm thick.
4) Average particle diameter is 65 nanometers.
5) Particle size distribution is narrow (50 nm FWHM) with no particles larger than 120 nm.
6) Passivated powder does not react in air up to at least 400 C.
7) Powder is extremely pure, typically 73% Mg and 27% O, with less than 0.1 atomic percent impurities.

Copper:

1) Particle morphology is roughly spherical.
2) Average particle diameter is approximately 10 nm.
3) Particle size distribution is very narrow (3 nm FWHM), with no particles larger than 17 nm.
4) Minimal (<2%) passivation was achieved on these particles, no distinct passivation layer is observed.
5) Powder is not pyrophoric, even without passivating layers present.
6) Some necking between particles is present, due, most likely, to the absence of particle passivating layers.
7) Powder is extremely pure, typically 98% Cu and 2% O, with less than 0.1 atomic percent impurities.

The experimental data supporting these observations are presented and described in detail in Section II.

SECTION II

Laboratory-scale apparatus

Our laboratory-scale furnace design for the dynamic gas condensation apparatus is shown in Fig. 1. The furnace incorporates three stages: a high temperature stage, a powder passivation stage, and a powder collection stage. A schematic diagram of the apparatus is shown in Fig. 2. Each of the three stages is described below.

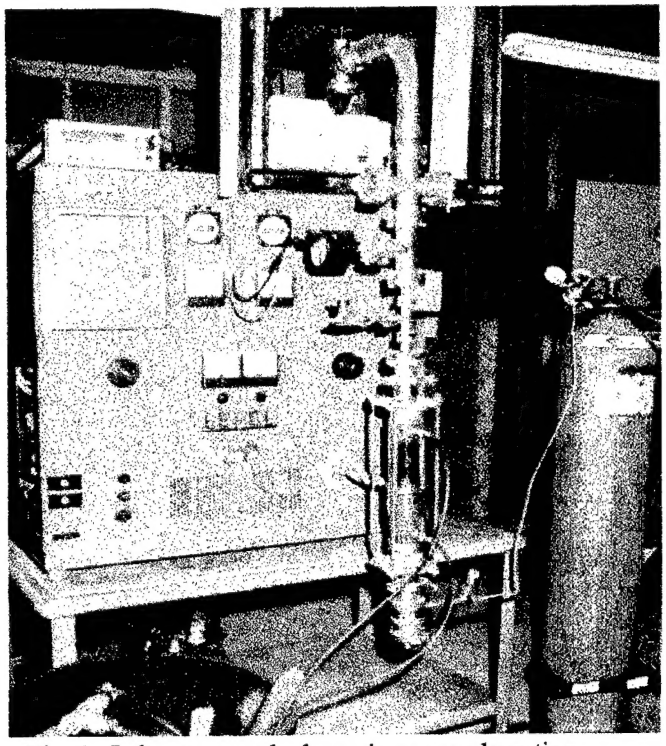

Fig. 1. Laboratory-scale dynamic gas condensation apparatus.

The high temperature stage, shown in Fig. 3, consists of a 1"-diameter x 1.5"-long x 0.5"-thick, pyrolytic-graphite annular ring that serves as a heating susceptor and holder for one or more 1/4" diameter BN crucibles that contain the bulk metal that is to be converted into nanometer powder. The susceptor/crucible assembly is oriented vertically and supported by a 0.25" diameter alumina tube from the bottom. The assembly is positioned inside, and midway up, a 1.5"-ID x 15"-long vertical glass tube. The glass tube is attached to

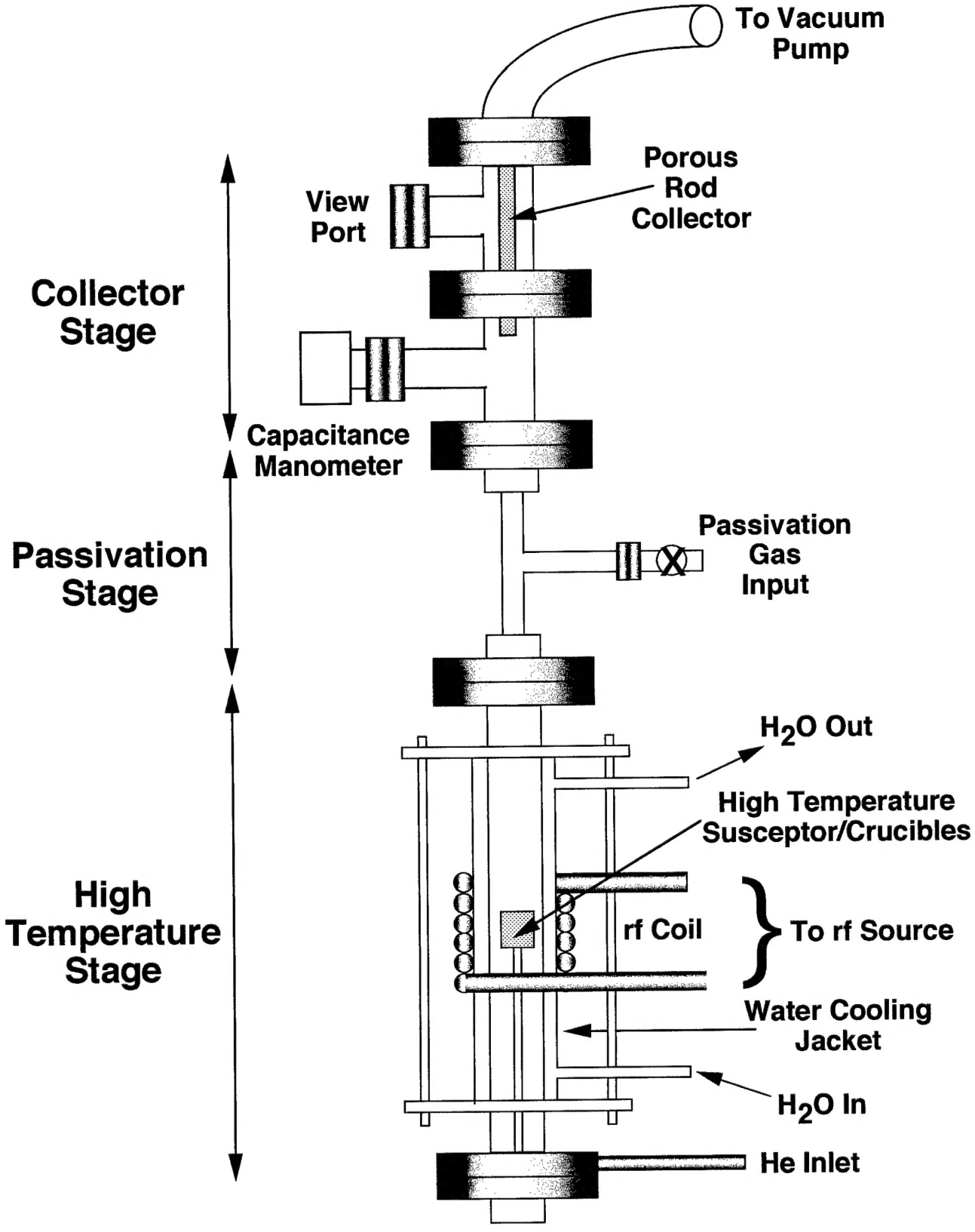

Figure 2. Induction furnace assembly constructed for the laboratory-scale production of nanometer-scale metal powders using dynamic gas condensation.

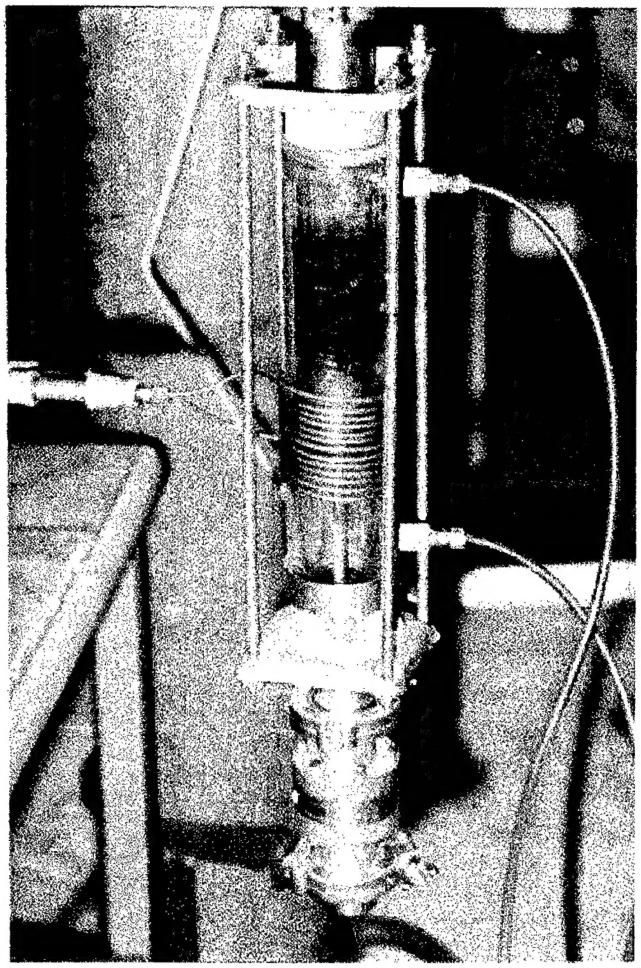

Fig. 3. High temperature stage of the dynamic gas condensation apparatus.

the powder passivation stage at the top and a terminating gas inlet flange at the bottom and is surrounded by a plastic water cooling jacket with 1/4" polyflow inlet and outlet connectors. The interior of the glass tube assembly is sealed from the outside atmosphere and cooling water with multiple viton o-rings but is open to the passivation stage. A water-cooled, copper coil (initially 6 turns, 1/4" tubing) is connected to the rf power source and surrounds the water jacket such that the crucibles are in the center of the coil. Helium gas is injected at the bottom of the high temperature stage and flows upward through the furnace at 1.5 SCFM to a vacuum pump that is connected to the top of the powder collector stage. The vacuum pump maintains 13 Torr of steady-state pressure in the system during flow conditions.

The powder passivation stage is constructed of 0.75" diameter stainless steel tubing and creates a high-velocity gas flow field into which an oxidizer gas (air, in the initial tests) can be injected into the helium stream. The high-velocity flow region minimizes backflow contamination of the high-temperature stage with oxidizer gas. This feature is necessary to prevent pre-oxidation of the metal particles that form in the high-temperature stage. Particles that have formed in the high-temperature stage are carried by the helium stream through the passivation stage where reaction with the oxidizer gas forms a passivation coating on each particle as it transits the stage enroute to the powder collector stage. Passivation layer thickness on each particle is controlled by the level of injection of the oxidizer gas. For air as the oxidizer, the level of injection is nominally set to be 2% of the steady-state pressure in the furnace to achieve adequate passivation.

The powder collector stage, shown in Fig. 4, is constructed of several sections of 1.5" diameter stainless steel tubing that contains a 6"-long x 0.75"-diameter, porous-nickel collecting rod. The porous (vertical) collector rod can be seen through the viewport in Fig. 4. Helium flows through the collector stage, through the porous rod to the vacuum pump. Metal nano-particles that are entrained in the helium flow collect on the exterior surfaces of the porous rod but do not pass through to the interior of the rod. Pore

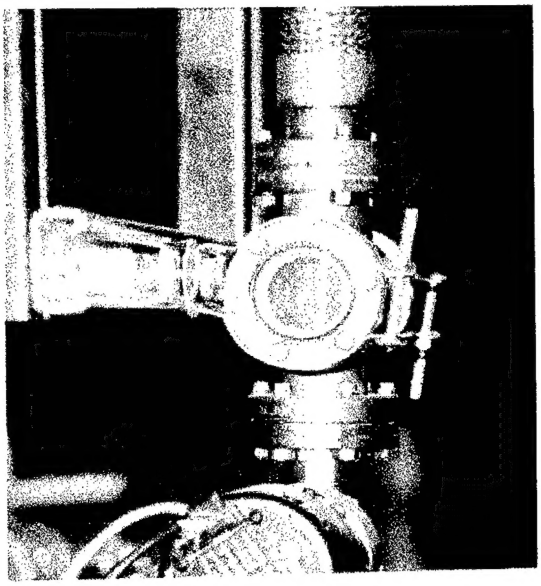

Fig. 4. Collector stage of the dynamic gas condensation apparatus.

diameters of the nickel rod are approximately 20 micrometers and are non-line-of-sight into the interior of the rod. The collected metal powder is easily removed from the exterior of the rod by gentle scraping or moderate vibration.

Nanometer-scale metal powder analyses

We utilized User Facilities at Los Alamos National Laboratory to analyze our powders. For electron microscopy, we used a state-of-the-art, field-emission JEOL model 3000-F transmission electron microscope to determine particle morphology, particle size, particle size distribution, and passivation layer structural characteristics of the metal-powder particles. The microscope was operated at 300 kV accelerating potential and provides image magnifications in the 100,000-300,000 range with 0.1 nanometer (1 angstrom) resolution. In addition, we used a National Electrostatics tandem accelerator to provide high-energy ions for standard Rutherford backscattering and nuclear resonance measurements. The ion scattering measurements were used to determine elemental purity in the metal powders to less than 0.1 atomic percent concentrations with an absolute accuracy of 5%. Helium ions (alpha particles) at 2.0 MeV and 7.6 MeV are used in the ion scattering measurements; 2.0 MeV for RBS measurements to determine majority and minority elemental levels and 7.6 MeV for nuclear resonance measurements to determine the magnitude of low-level oxygen concentrations in the copper powder. Oxygen is directly observable in the RBS spectra for the aluminum and magnesium powders but not for the copper powder. Thus, standard RBS measurements are sufficient to determine oxygen concentration in the aluminum and magnesium powders but not in the copper powder. To determine oxygen content in the copper powder, we employed a nuclear resonance technique[1] to enhance measurement sensitivity to oxygen by more than two orders of magnitude over the Rutherford (kinematic) scattering value.

Aluminum

Samples were prepared for TEM analysis by 1) mixing a small amount of the nanometer-scale, bulk aluminum powder with hexane to form a pseudo-colloidal particle suspension (mud), 2) sonicating with ultrasound for 5 minutes (to break up any particle agglomerates), and 3) passing a standard TEM copper mesh grid (with holey carbon film) through the mixture to collect particles. The RBS samples were 1/4"-diameter disks (typically 0.020" thick) that were hand pressed from the bulk magnesium powder. Figures 5 & 6 are TEM micrographs of aluminum powders that were collected from the collecting rod assembly. The micrographs reveal that the typical particle morphology is roughly

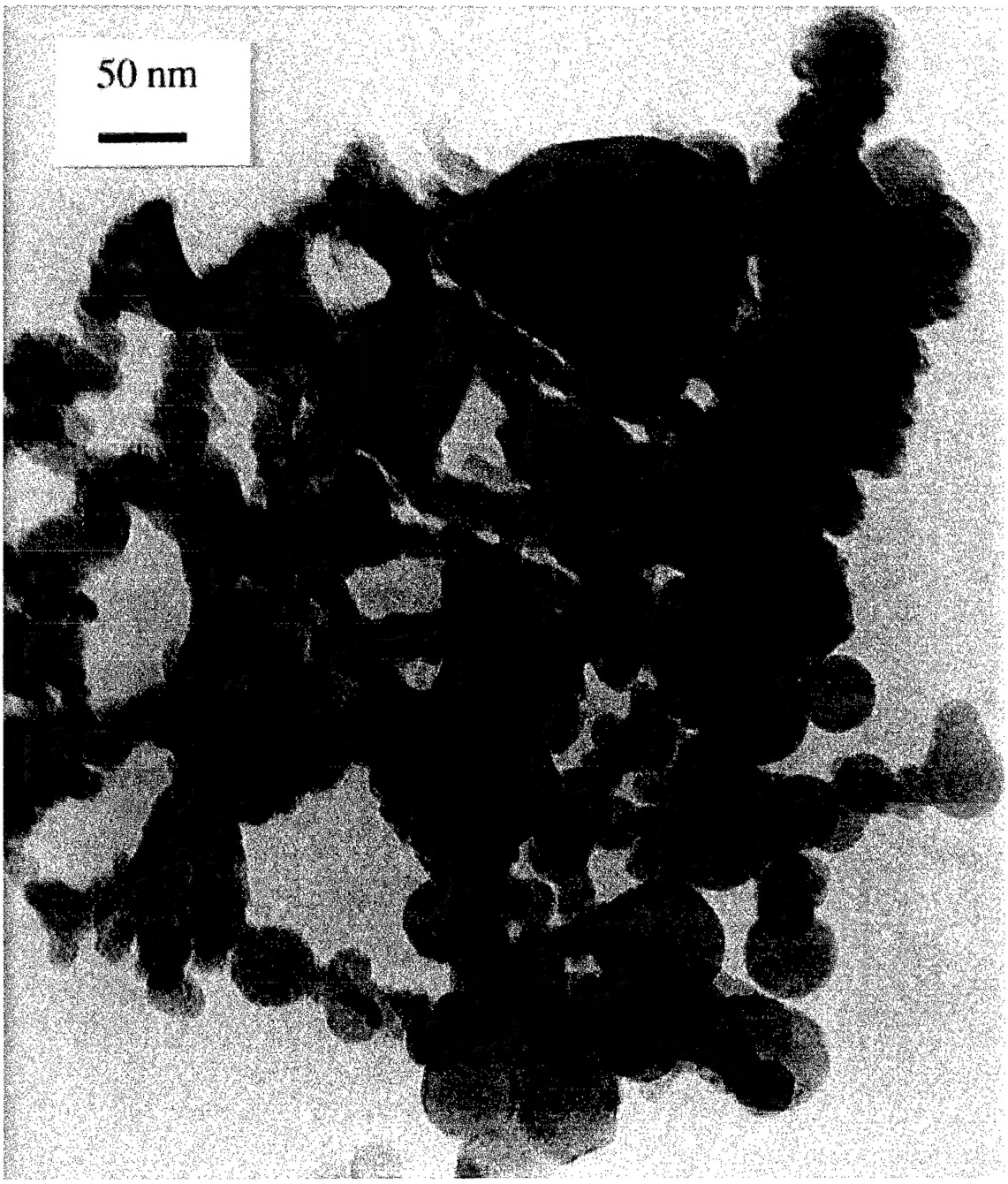

Figure 5. TEM micrograph of aluminum powder fabricated using dynamic gas condensation.

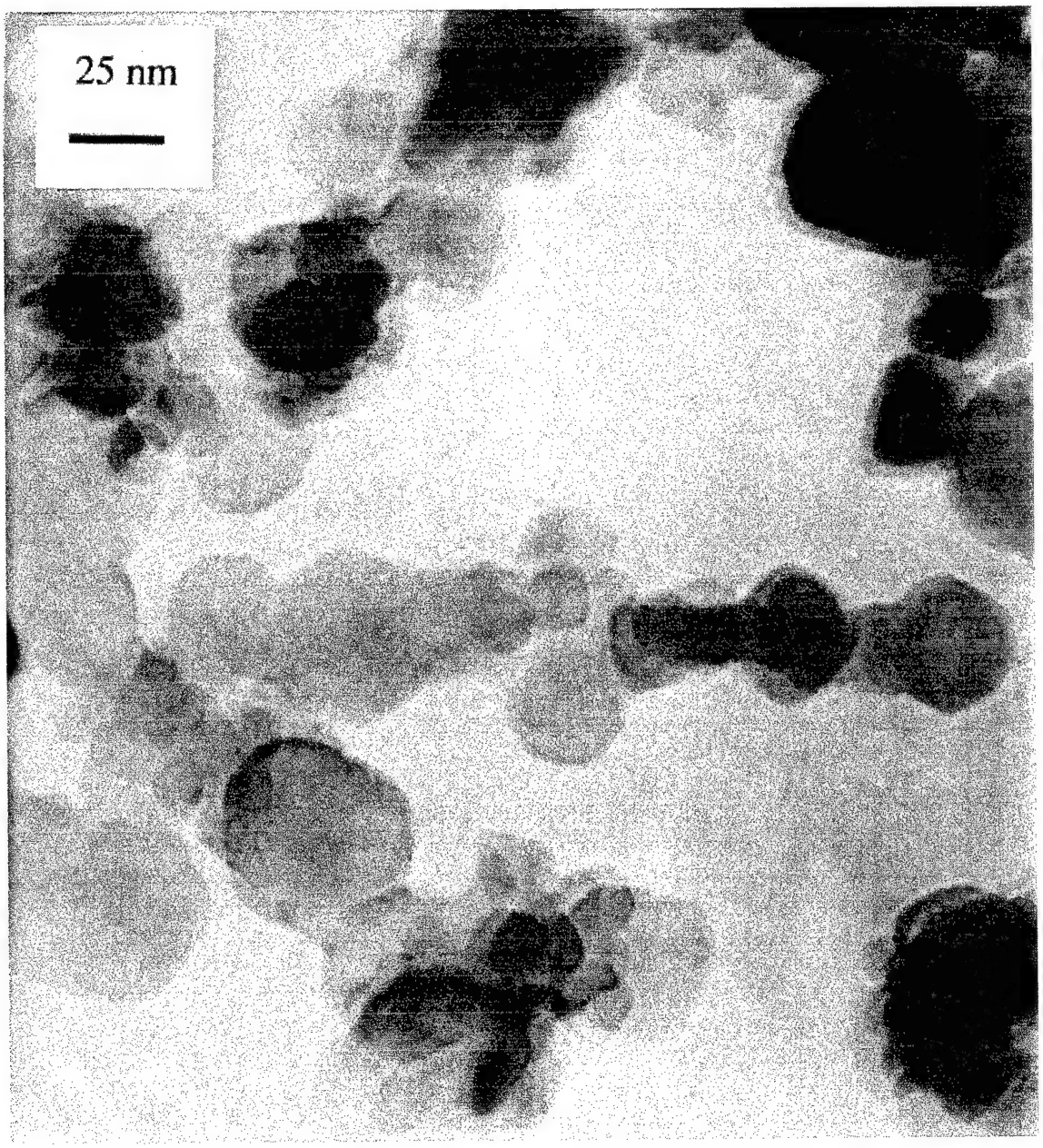

Figure 6. TEM micrograph of a second sample of aluminum powder that was fabricated using dynamic gas condensation.

spherical. The average particle size is 31 nanometers, determined from the measurements of 110 distinguishable particles in Figs. 5 & 6. Size calibration for the images are given by the horizontal calibration bars shown in each micrograph.

Size distributions for the aluminum powders that were collected from the collecting rod assembly are shown in Figure 7.

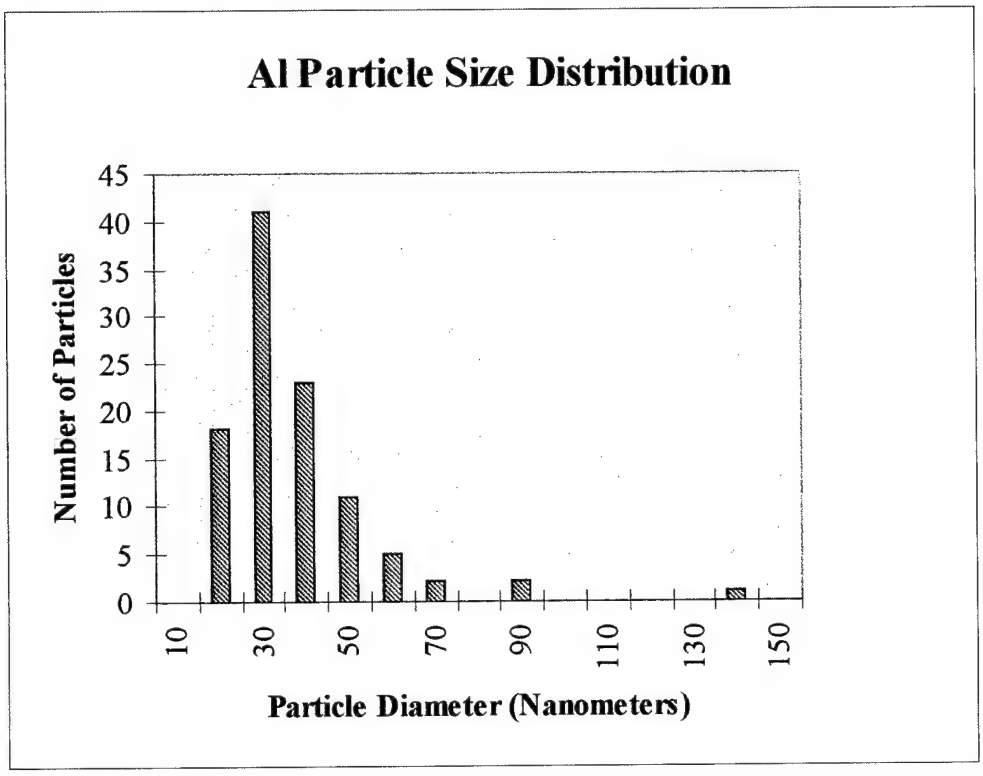

Figure 7. Size distribution for aluminum powders that were collected from the collecting rod assembly. The distribution is narrow and does not contain any sizes larger than 150 nanometers.

The aluminum powders consist of particles that are passivated with Al_2O_3. Figure 8 shows the TEM micrograph of a typical, passivated, aluminum particle. The image reveals that the passivation layer is approximately 3 nanometers thick. In addition, the image shows that the passivation layer is amorphous and the interior of the particle is crystalline.

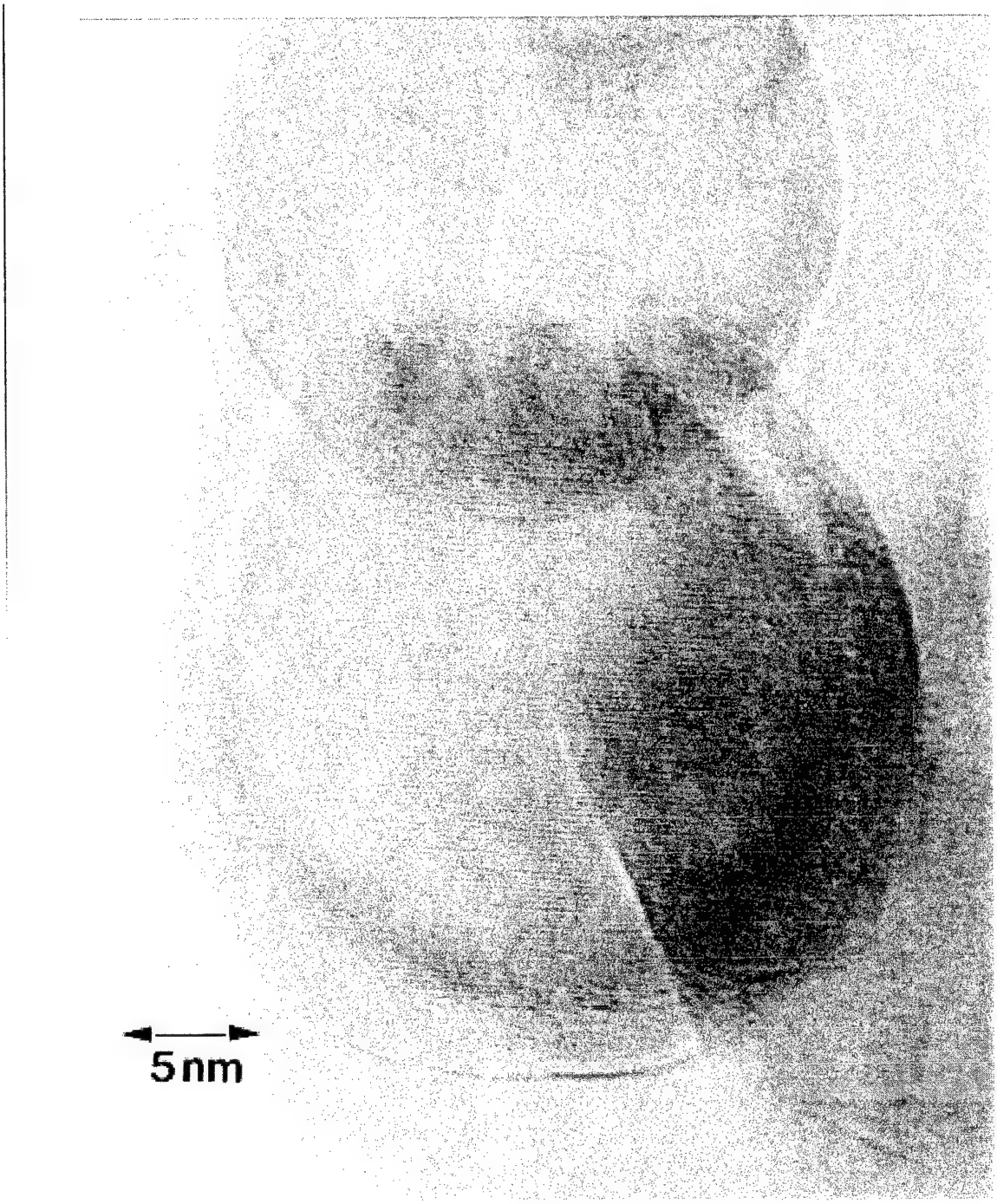

Fig. 8. TEM image of a passivated, aluminum nano-particle. The amorphous Al_2O_3 passivation layer is nominally 3 nanometers thick.

Absolute purity of the aluminum powder was determined using Rutherford backscattering spectrometry, as noted earlier. The technique is sensitive to all elemental

species that are heavier than helium. Figure 9 is the RBS spectrum from the aluminum powder. Absolute elemental concentrations were determined by matching a computer simulation of the spectrum with the experimental data. Elemental concentrations in the simulation are varied until the simulated spectrum matches the experimental spectrum. In the figure, the experimental data appear as individual points and the computer-simulated spectrum is shown as a solid line. Energy positions for backscattering events from surface species are shown in the figures. The relative heights of the steps are proportional to the elemental concentrations in the powders. The powders consist of aluminum and oxygen. All other elemental species are less than 0.1 atomic percent.

We observe that the Al_2O_3 layer on the aluminum particles is an effective passivating layer, as the powders are not pyrophoric after fabrication. In contrast, aluminum powder that was collected below the passivation section in the fabrication apparatus is pyrophoric. Further, we note that the passivated aluminum powder does not react when heated to moderate temperatures in air, even to 400 C. This is an important observation in that it supports the possibility that the passivated powder can be intimately mixed with a strong solid-state oxidizer (e.g., MoO_3) without ignition. Such metastable mixtures are similar to the Metastable Interstitial Composite (MIC) materials that are being produced at Los Alamos National Laboratory for a variety of energetic materials applications, including reactive fill for enhanced-lethality warheads, percussion ammunition primers, and solid rocket propellant additives.

Magnesium

Samples were prepared for TEM analysis by 1) mixing a small amount of the bulk magnesium powder with hexane to form a pseudo-colloidal particle suspension (mud), 2) sonicating with ultrasound for 5 minutes (to break up any particle agglomerates), and 3) passing a standard TEM copper mesh grid (with holey carbon film) through the mixture to collect particles. The RBS samples were 1/4"-diameter disks (typically 0.020" thick) that were hand pressed from the bulk magnesium powder.

Figures 10 and 11 are TEM micrographs of magnesium powders that were collected from the bottom region of the collecting rod assembly. The micrographs reveal that the typical particle morphology is right hexagonal. The average particle size is 61 nanometers, determined from the measurements of 110 distinguishable particles in Figs. 10 & 11. Size calibrations for the images are given by the white, horizontal bar at the bottom of each micrograph. Random orientations of the magnesium particles are observed in the figures. For illustration, a schematic diagram of a right hexagon is shown in Figure 12.

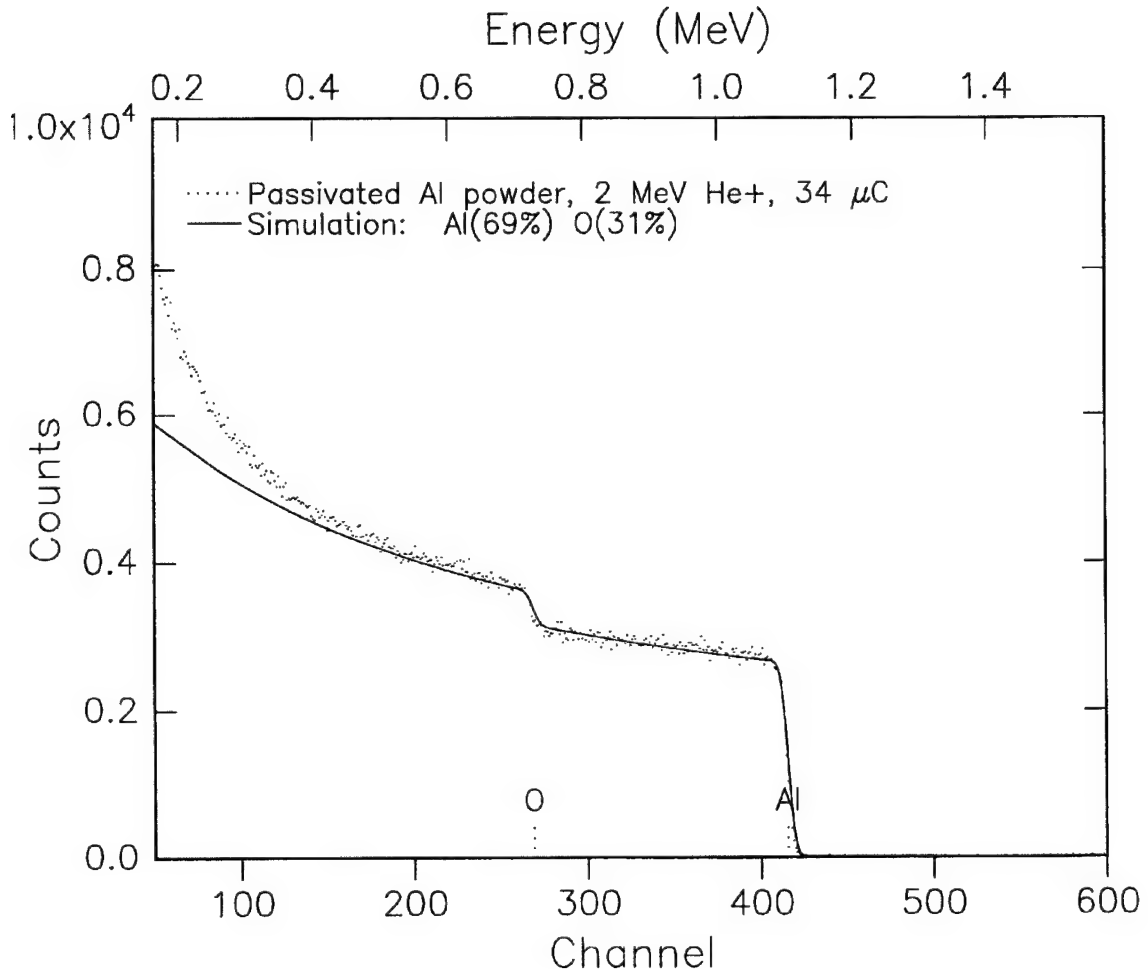

Figure 9. 2-MeV Rutherford backscattering measurement of a pressed pellet of passivated, nanometer-scale aluminum powder. Elemental contaminant levels are below 0.1 atomic percent.

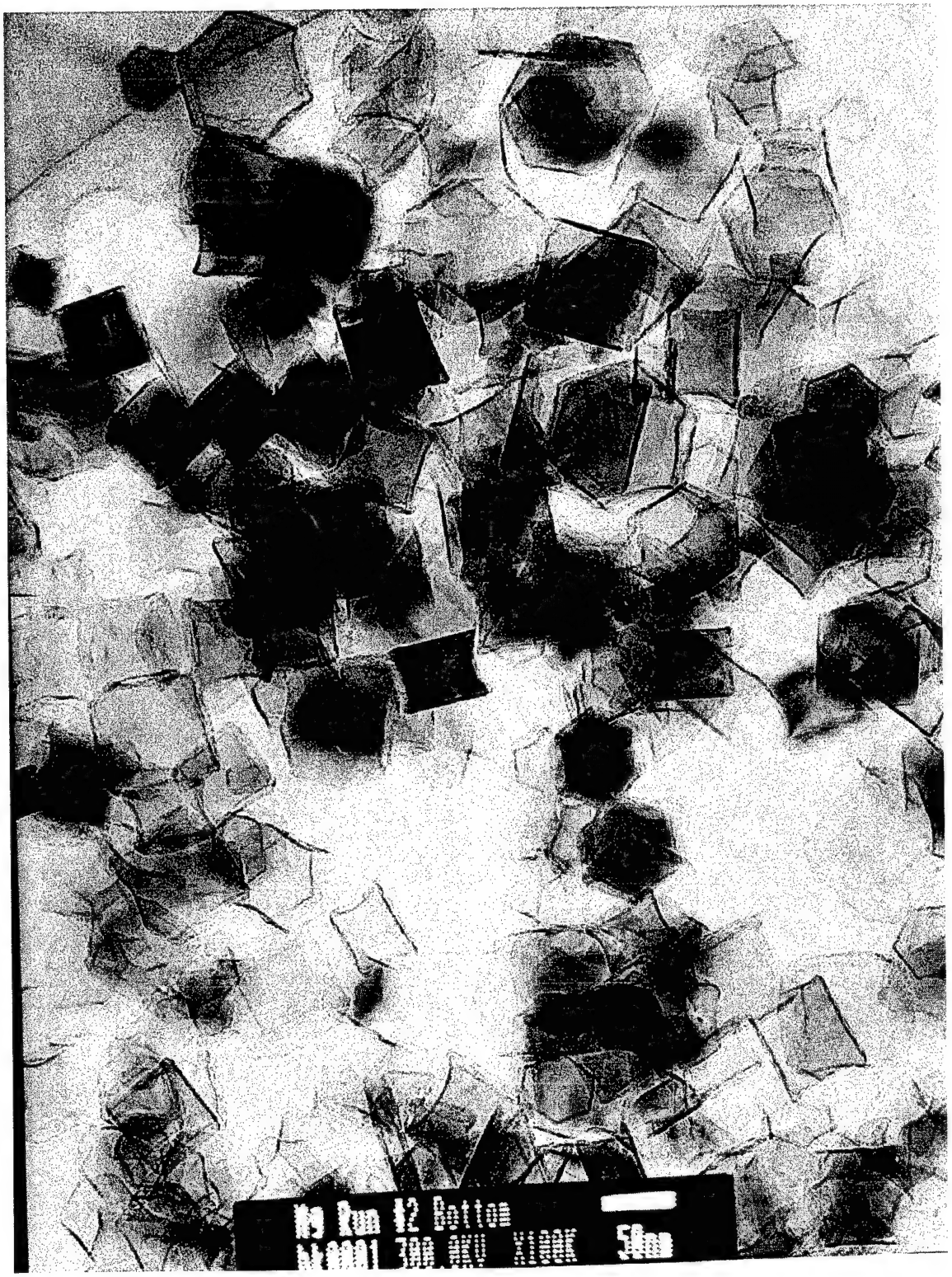

Figure 10. TEM micrograph of a sample of magnesium powder obtained from the bottom of the collecting rod. For calibration, the white bar at the bottom is 50 nanometers.

Figure 11. TEM micrograph of a second sample of magnesium powder obtained from the bottom of the collecting rod. For calibration, the white bar at the bottom is 50 nanometers.

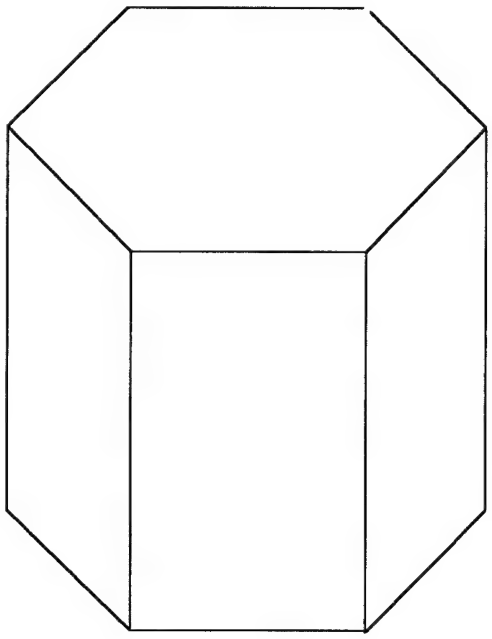

Figure 12. Particle morphology of the magnesium particles is that of a right hexagon, similar to that shown above. TEM micrographs of the magnesium powders show such particles in random orientations.

Figures 13 & 14 are TEM micrographs of magnesium powders that were collected from the top region of the collecting rod. No strong structural differences were noted between samples that were collected from top of the collecting rod versus those that were collected from the bottom. The average particle size is slightly larger for powders that are collected from the top, but not significantly so. Average particle size for the powders collected from the top region is 69 nanometers.

Size distributions for the magnesium powders that were collected from both top and bottom regions of the collecting rod assembly are shown in Figure 15.

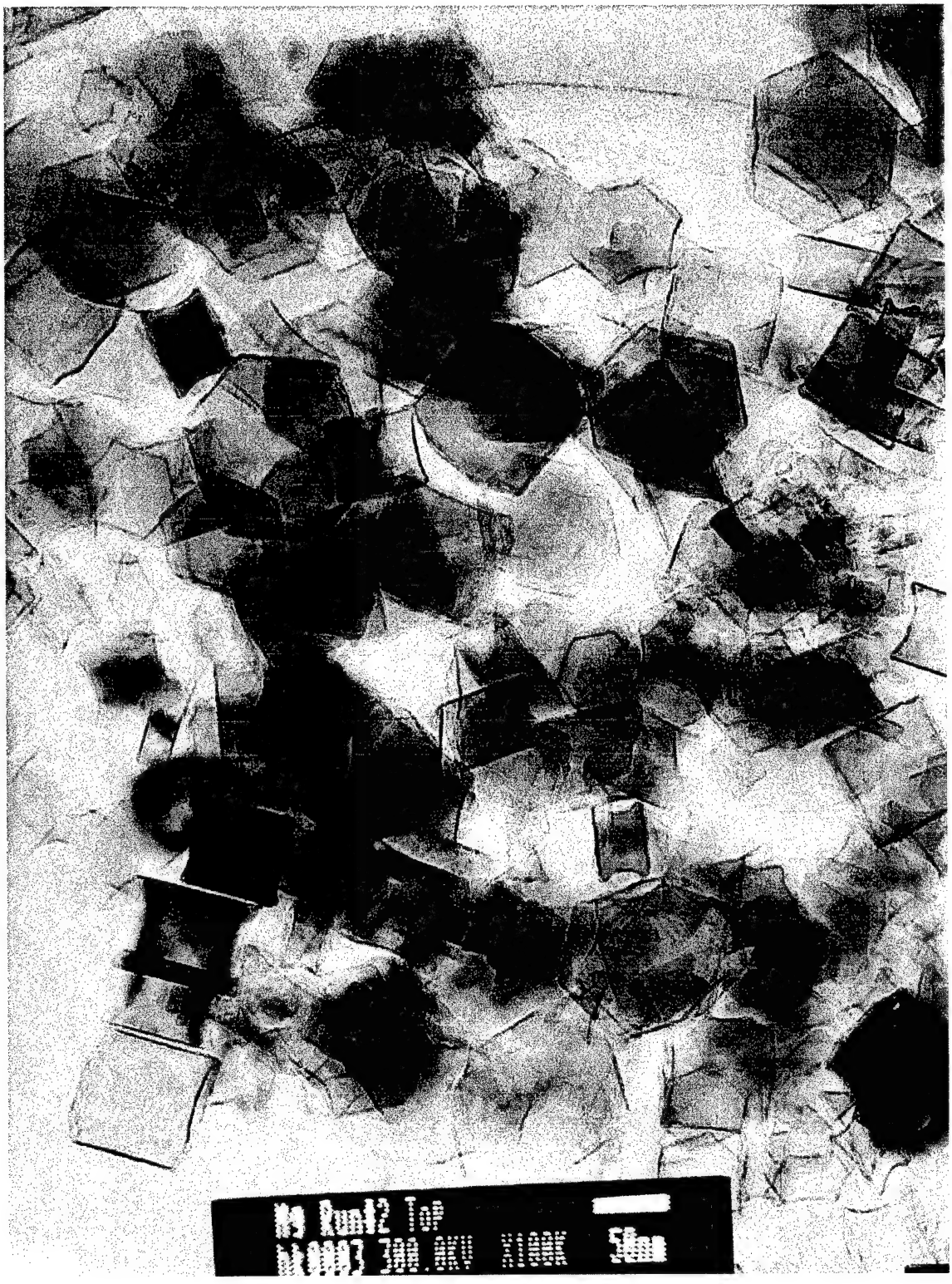

Figure 13. TEM micrograph of a sample of magnesium powder obtained from the top region of the collecting rod. For calibration, the white bar at the bottom is 50 nanometers.

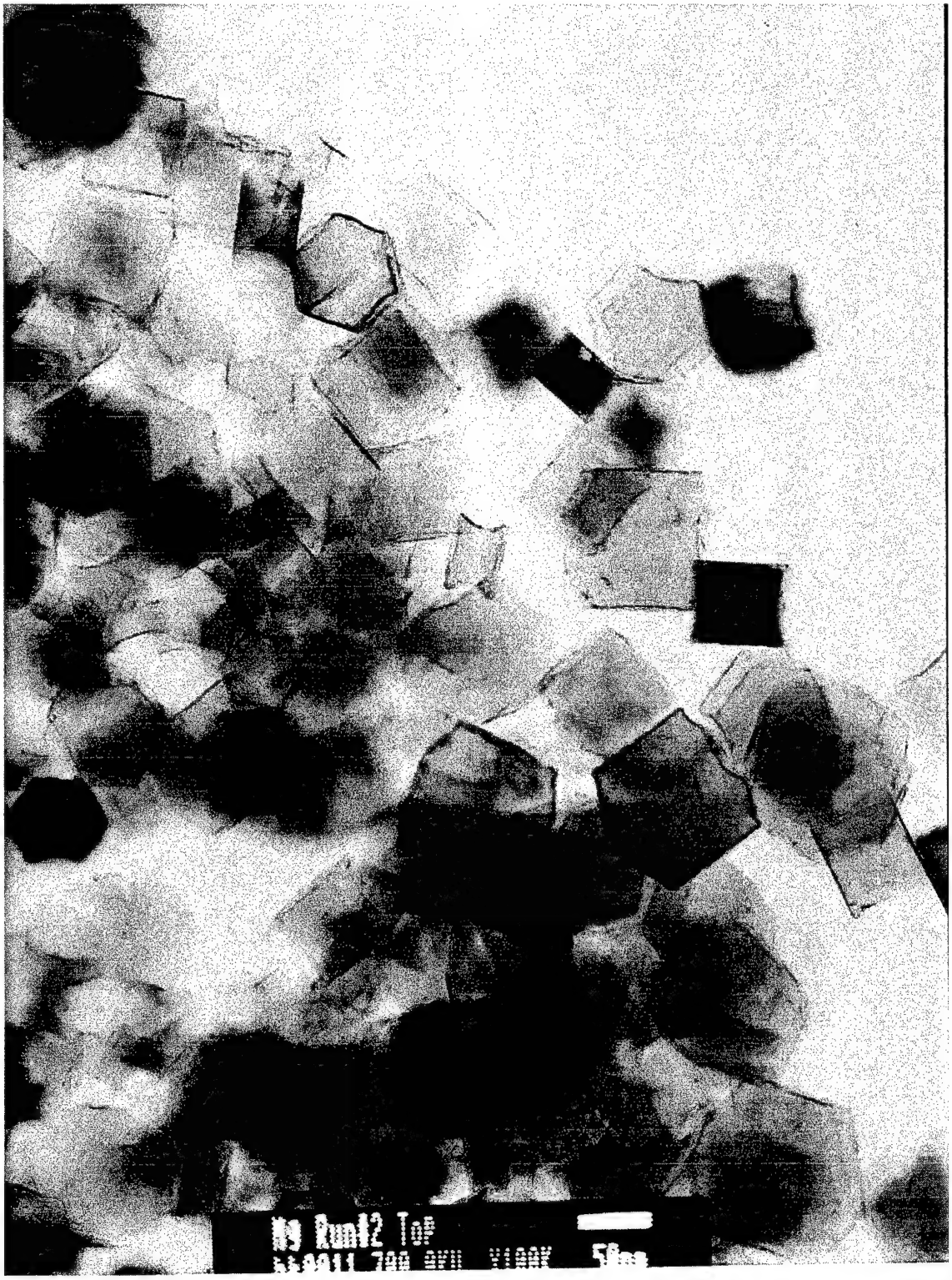

Figure 14. TEM micrograph of a second sample of magnesium powder obtained from the top region of the collecting rod. For calibration, the white bar at the bottom is 50 nanometers long.

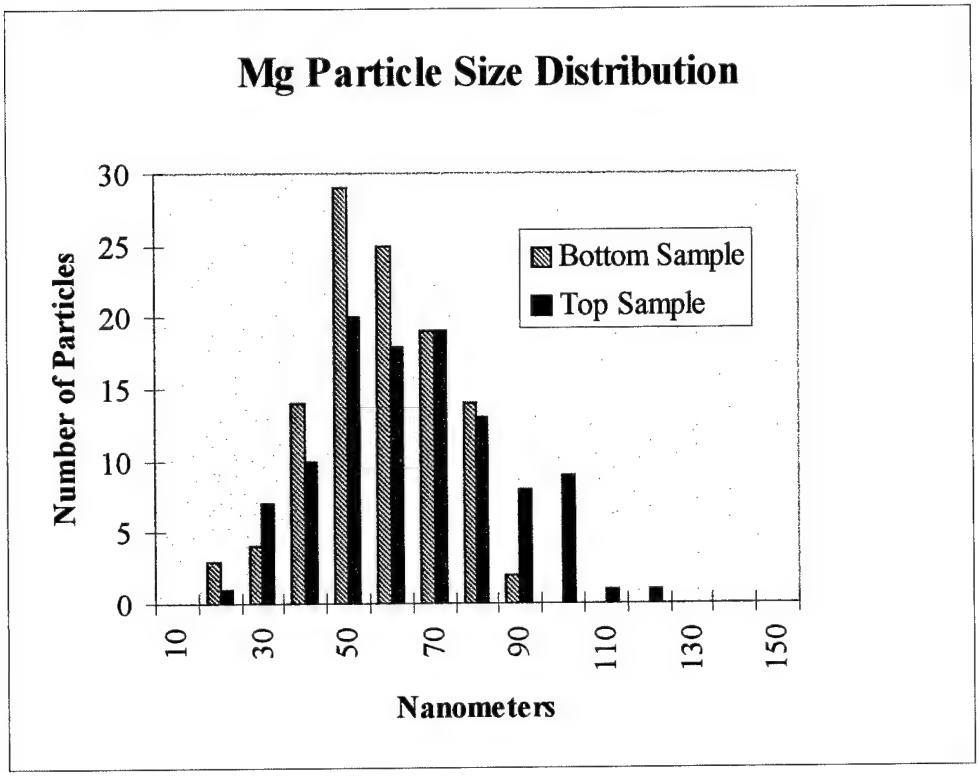

Figure 15. Size distributions for magnesium powders that were collected from the top and bottom regions of the collecting rod assembly. Distributions are narrow and do not contain any sizes larger than 130 nanometers.

The magnesium powders consist of particles that are passivated with MgO. Figure 16 shows the TEM micrograph of a typical, passivated, magnesium particle. The image reveals that the passivation layer is approximately 2.5 nanometers thick. In addition, the image shows that both the passivation layer and the interior of the particle are crystalline.

Absolute purity of the magnesium powder was determined using Rutherford backscattering spectrometry, as noted earlier. The technique is sensitive to all elemental species that are heavier than helium. Figures 17 & 18 are RBS spectra of the magnesium powders that were collected from the bottom and top regions, respectively, of the collecting rod assembly. Absolute elemental concentrations in the samples were determined by matching a computer simulation of the spectrum with the experimental data. Elemental concentrations in the simulation are varied until the simulated spectrum matches the experimental spectrum. In both figures, the experimental data appear as individual points and the computer-simulated spectrum is shown as a solid line. Energy positions for backscattering events from surface species are shown in the figures. The relative heights of the steps are proportional to the elemental concentrations in the powders. The powders consist of magnesium, oxygen, and a small concentration (0.06 at.%) of calcium. All other elemental species are less than 0.1 atomic percent. We note a

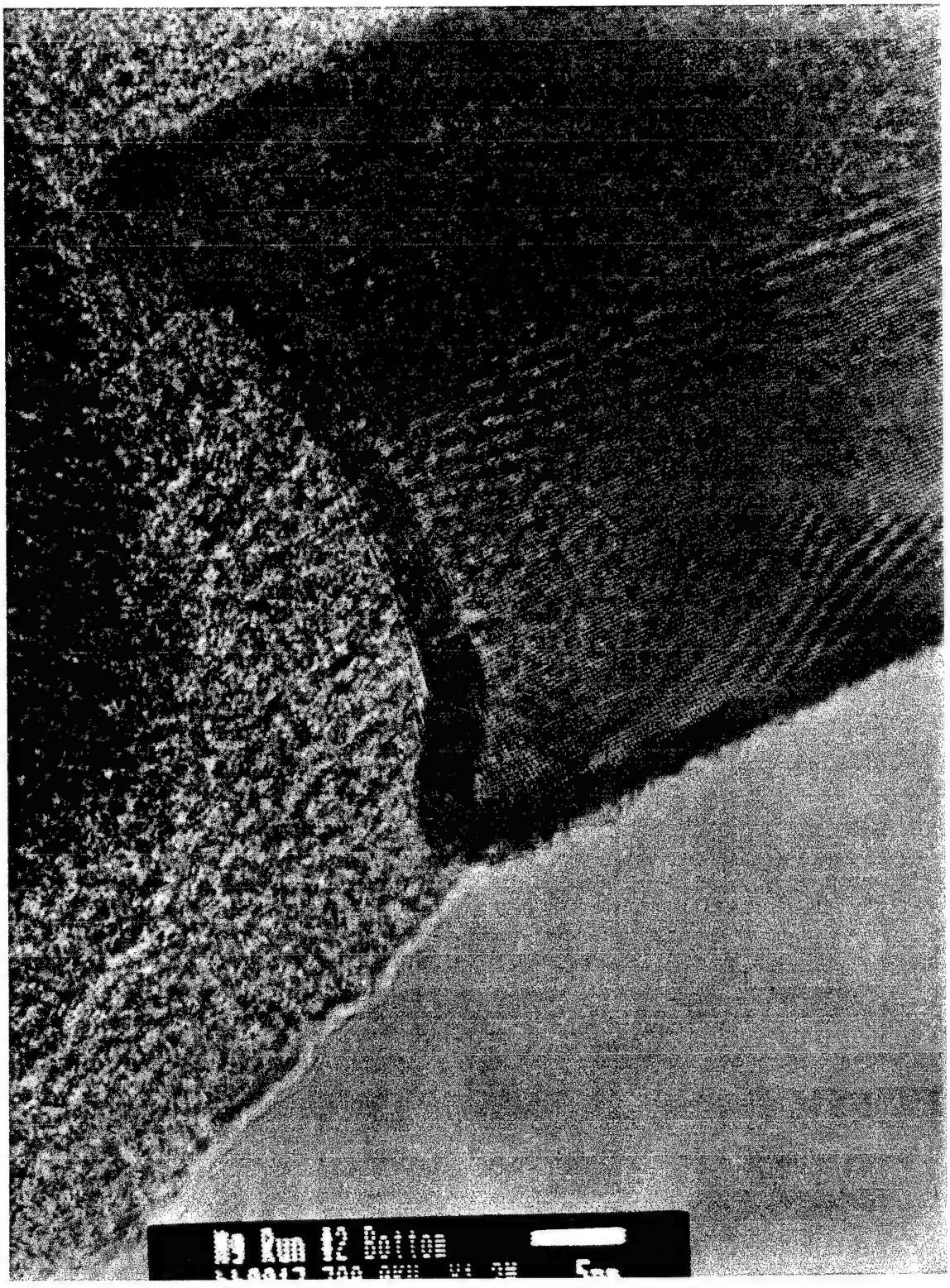

Figure 16. TEM micrograph of a passivated magnesium powder particle. The passivation layer consists of crystalline MgO, 2.5 nm thick (nominal). Particle interior is crystalline magnesium. The white bar at the bottom of the micrograph is 5 nanometers long.

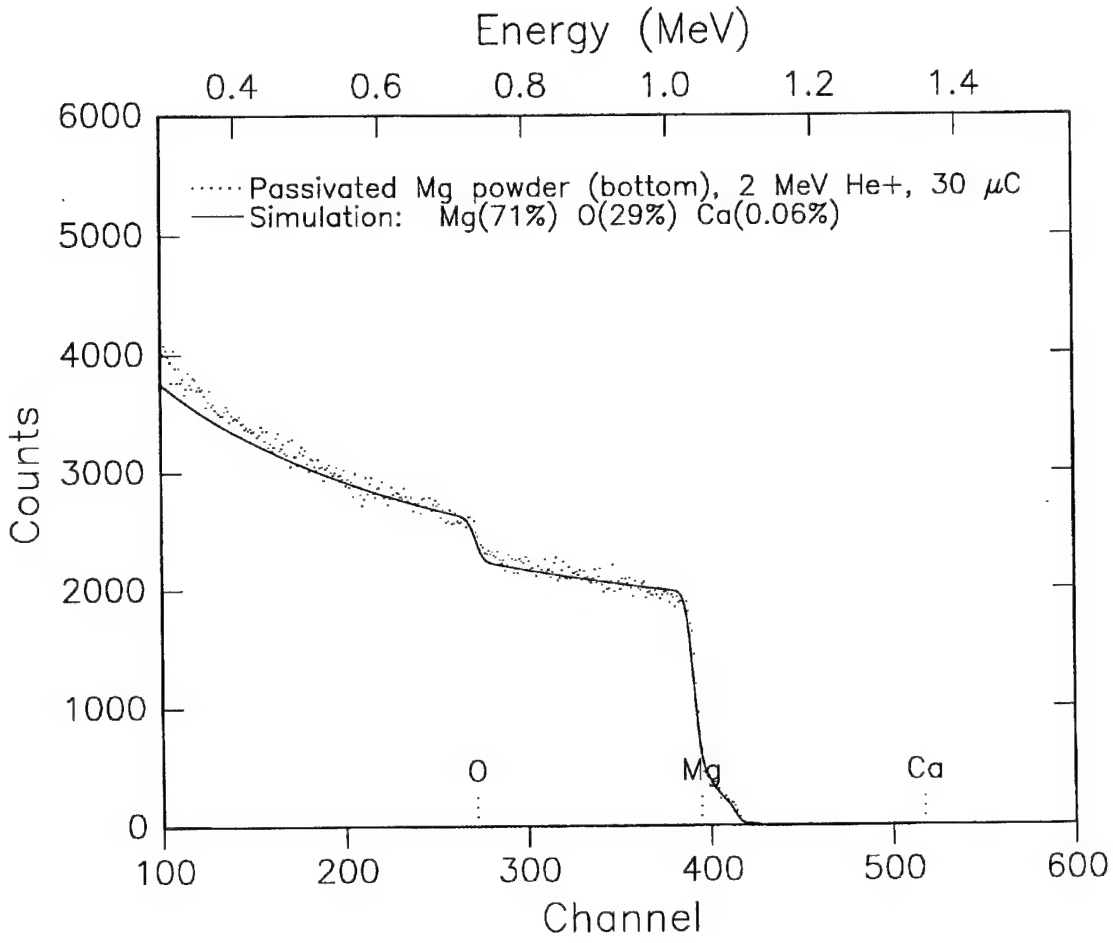

Figure 17. RBS spectrum from a hand-pressed pellet of passivated, nanometer-scale magnesium powder that was collected from the bottom region of the collecting rod assembly. Energy positions for surface backscattering for several elements are shown. Elemental concentrations are in atomic percent and are determined by matching a computer simulation (solid line) with the measured data (points). The magnesium to oxygen ratio in powder that is collected from the bottom region of the rod assembly is slightly lower than that for powder that is collected from the top region of the rod (see Fig. 18). See text for discussion. The spectrum reveals that the passivated magnesium powders are pure, with contaminant concentrations less than 0.1 atomic percent.

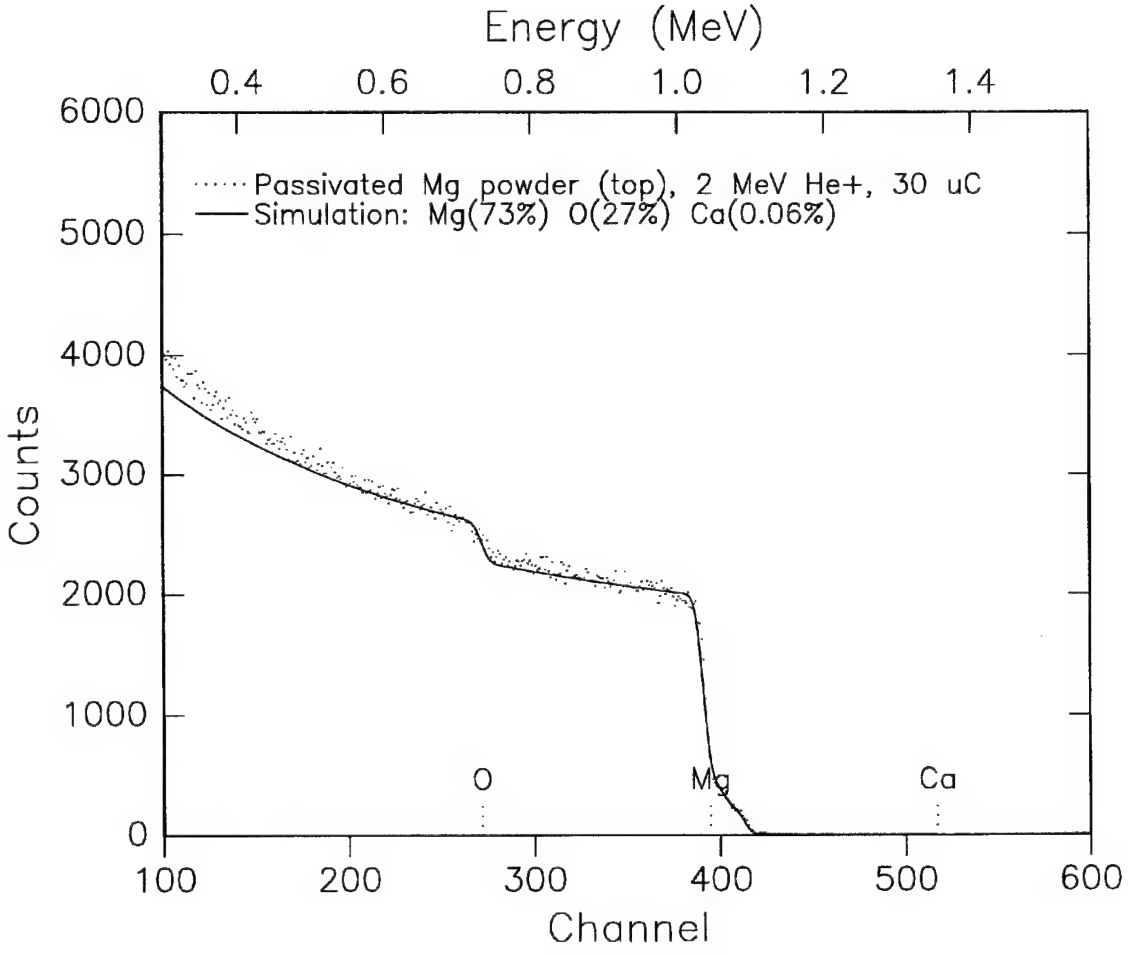

Figure 18. RBS spectrum from a hand-pressed pellet of passivated, nanometer-scale magnesium powder that was collected from the top region of the collecting rod assembly. The magnesium to oxygen ratio in powder that was collected from the top region of the rod assembly is slightly greater than that for powder collected from the bottom region of the rod (see Fig. 17).

slight increase in the magnesium concentration in powders collected from the top region of the collecting rod assembly; 73% Mg for particles from the top region versus 71% Mg for particles collected from the bottom. This observation is consistent with the TEM-based observation that the average particle size is slightly larger for powders collected from the top regions of the collecting rod. This result is understood by considering that, with a fixed passivation-layer thickness, the ratio of interior (metal) volume to passivation-layer (metal-oxide) volume is greater for a large than for a small particle. Thus, the ratio of magnesium to oxygen is larger for larger particles than the magnesium to oxygen ratio for smaller particles.

We observe that the MgO layer on the magnesium particles is an effective passivating layer, as the powders are not pyrophoric after fabrication. In contrast, magnesium powder that was collected below the passivation section in the fabrication apparatus is pyrophoric. Further, we note that the passivated magnesium powder does not react when heated to moderate temperatures in air, even to 400 C. This is an important observation in that it supports the possibility that the passivated powder can be intimately mixed with a strong solid-state oxidizer (e.g., MoO_3) without ignition. Such a metastable mixture would constitute a magnesium analog of the aluminum-based MIC materials that are being produced at Los Alamos National Laboratory for a variety of energetic materials applications, including reactive fill for enhanced-lethality warheads, percussion ammunition primers, and solid rocket propellant additives.

Copper

Samples were prepared for TEM and RBS analyses using the techniques that we described earlier for aluminum and magnesium. Figures 19 and 20 are TEM micrographs of copper powders that were collected from the bottom of the collection rod assembly. Figures 21 and 22 are similar micrographs of samples collected from the top of the collection rod assembly. No significant differences are observed between particles collected from the top of the collection rod versus those collected from the bottom. The micrographs reveal that the copper powder particle morphology is roughly spherical. Some necking between particles is observed and most of the particles do not appear to have a passivation layer. The necking is likely related to the minimal degree of passivation that was achieved. Necking can occur between unpassivated particles, if the particles are deposited together before sufficient cooling has occurred. Figure 23 shows that no clear passivation layer has been formed on the particles.

The average particle size for the copper powders is near 10 nanometers, with no large particles present. The particle size distributions for samples collected from the bottom and top of the collection rod are shown separately in Figure 24. The distributions were obtained from measurements of at least 110 individual particles for each sample type (top or bottom) shown in Figs. 19-22. The particle size distributions for the copper powders are extremely narrow: approximately 3 nm FWHM.

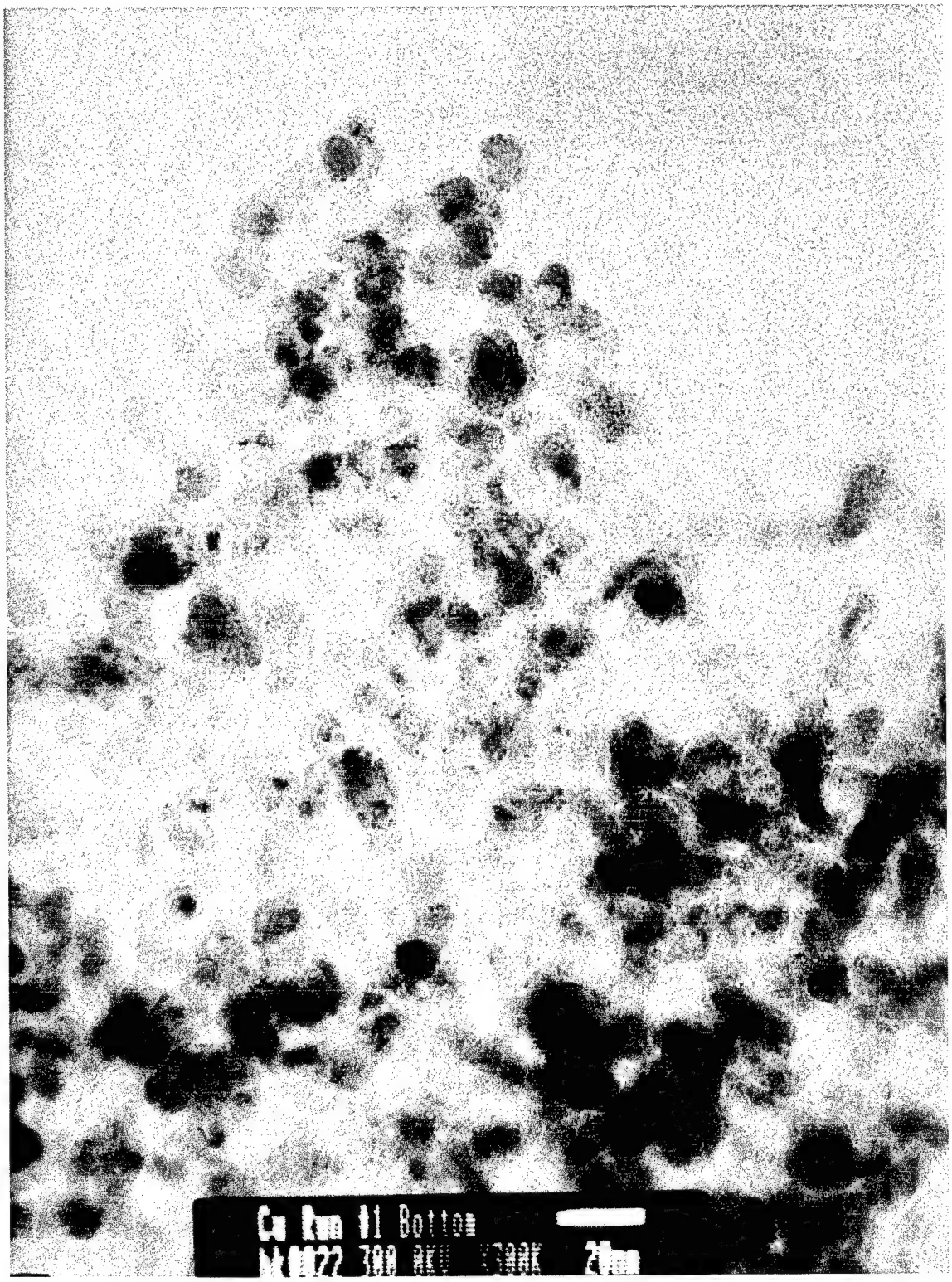

Figure 19. TEM micrograph of a sample of copper powder that was collected from the bottom portion of the collection rod. Average particle size is 10 nm. No passivation layer is evident.

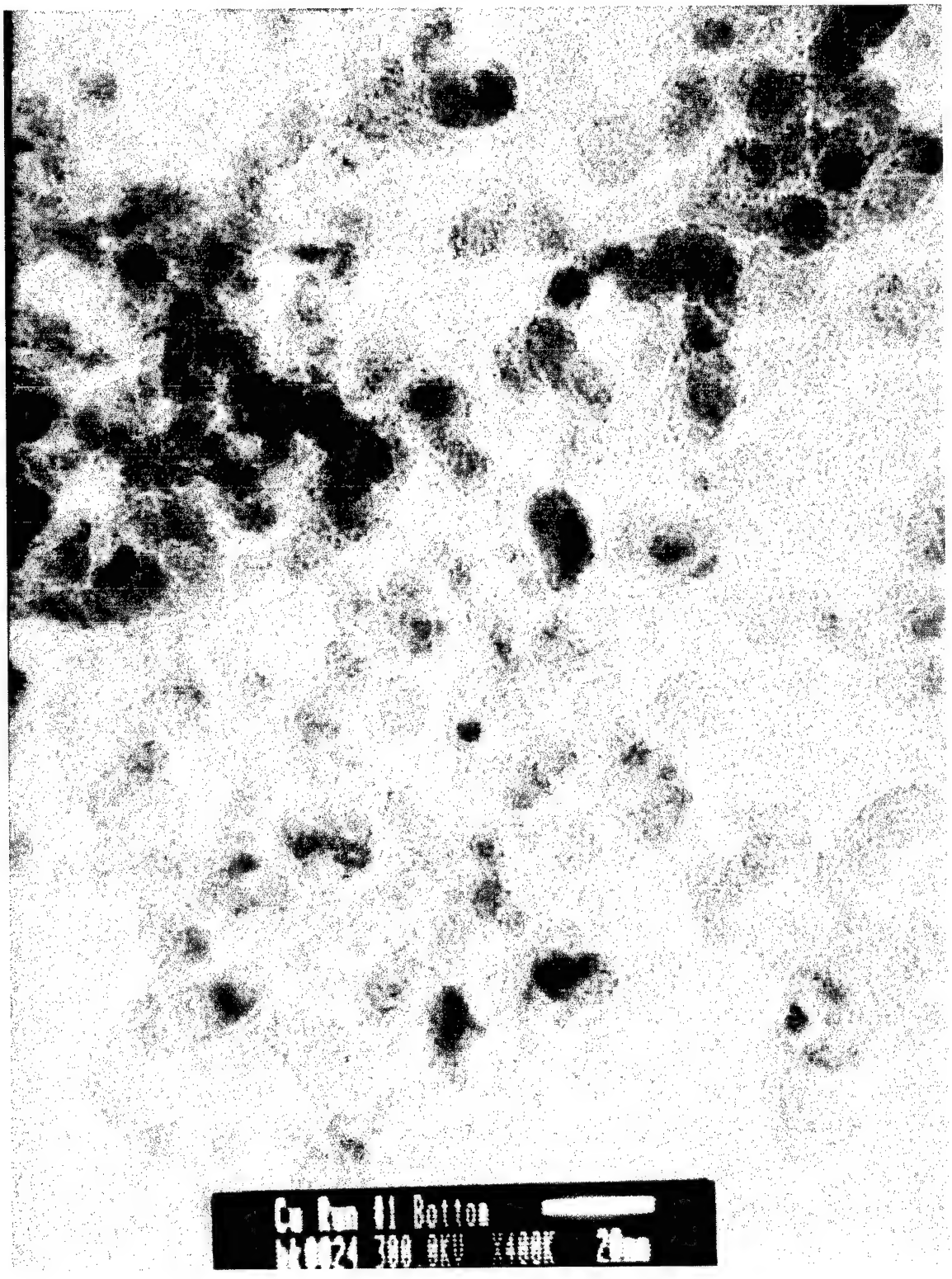

Figure 20. TEM micrograph of a second sample of copper powder that was collected from the bottom portion of the collection rod. The white bar length is 20 nm.

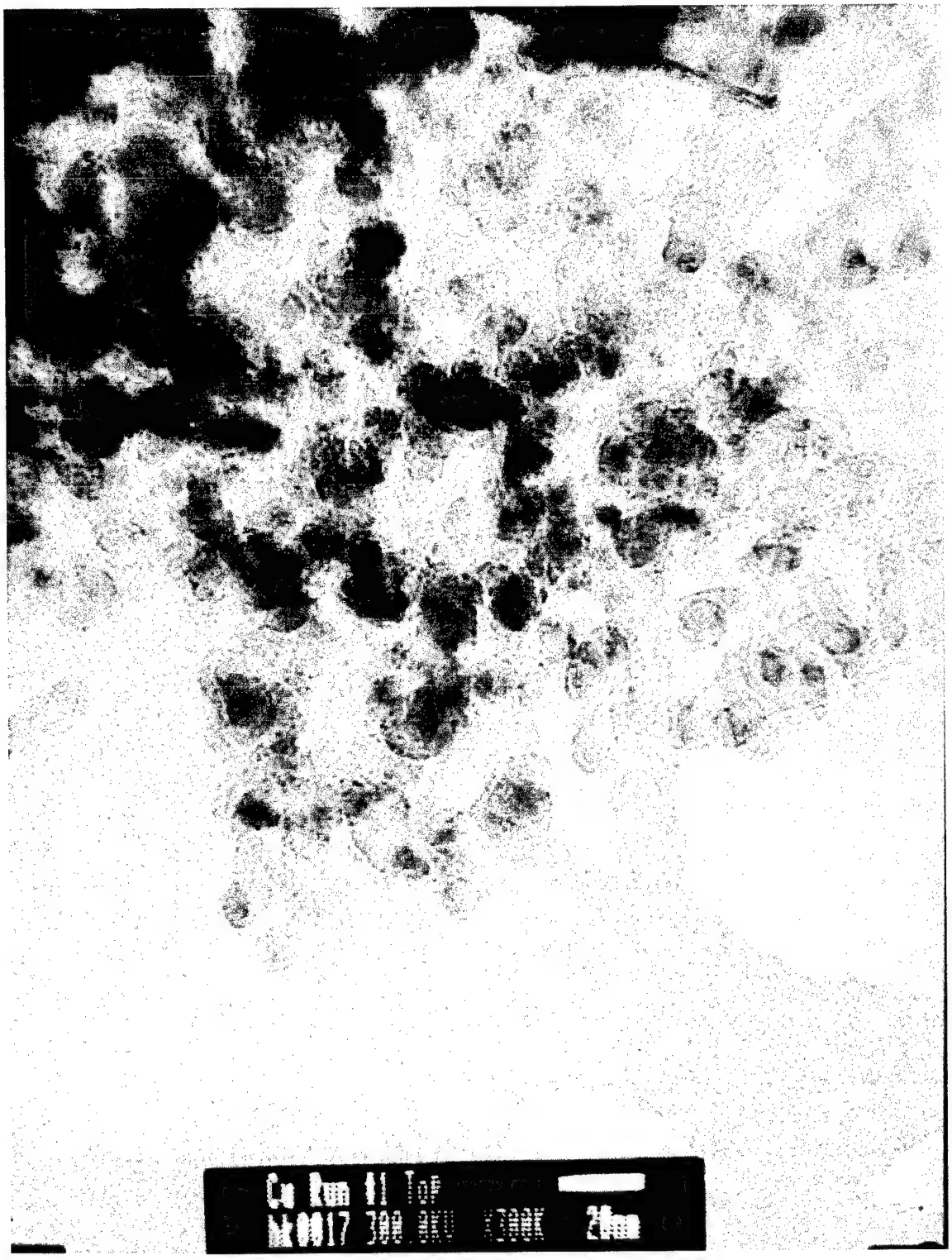

Figure 21. TEM micrograph of a sample of copper powder that was collected from the top portion of the collection rod. The white bar length is 20 nm.

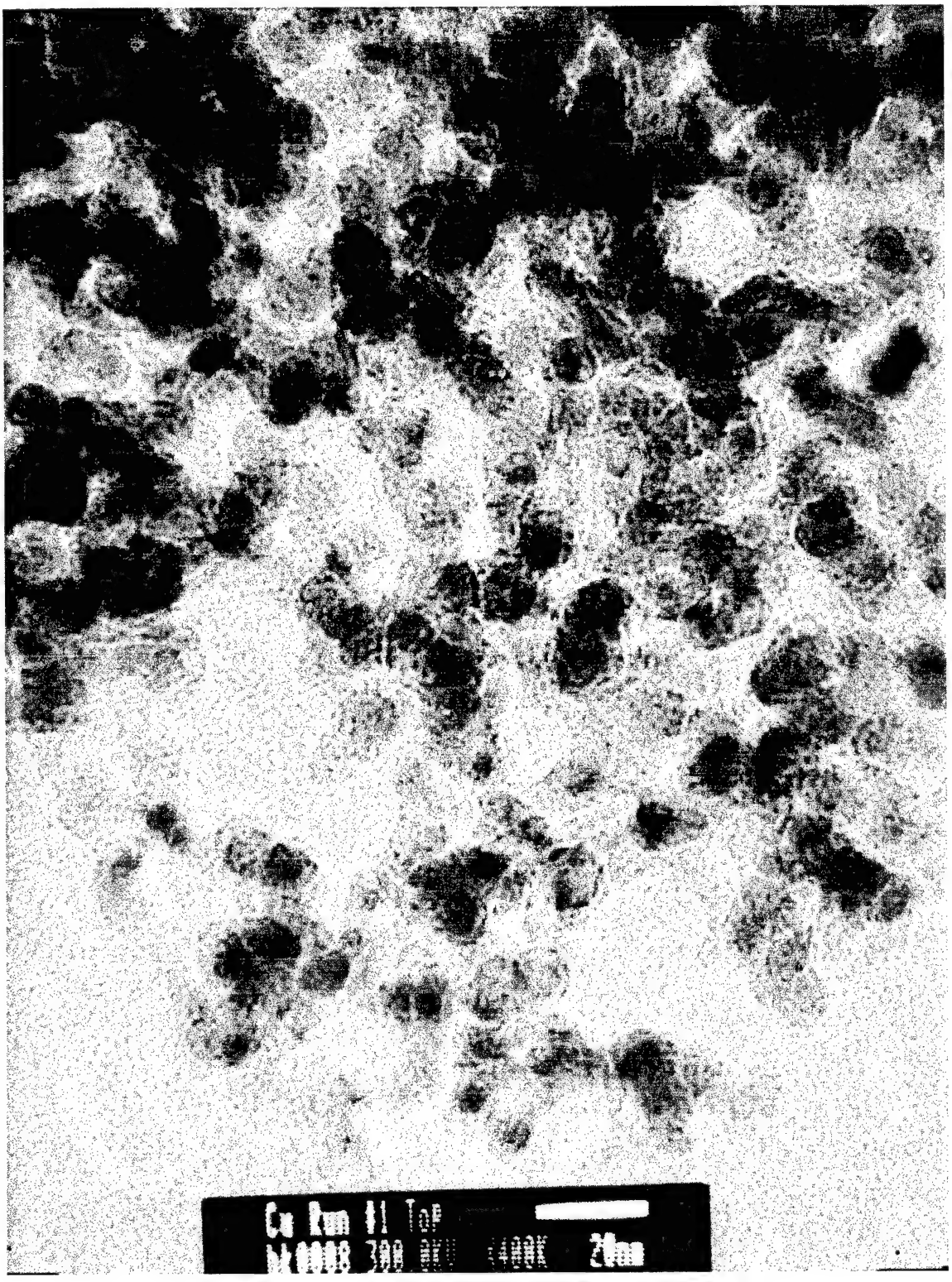

Figure 22. TEM micrograph of a second sample of copper powder that was collected from the top portion of the collection rod. The white bar length is 20 nm.

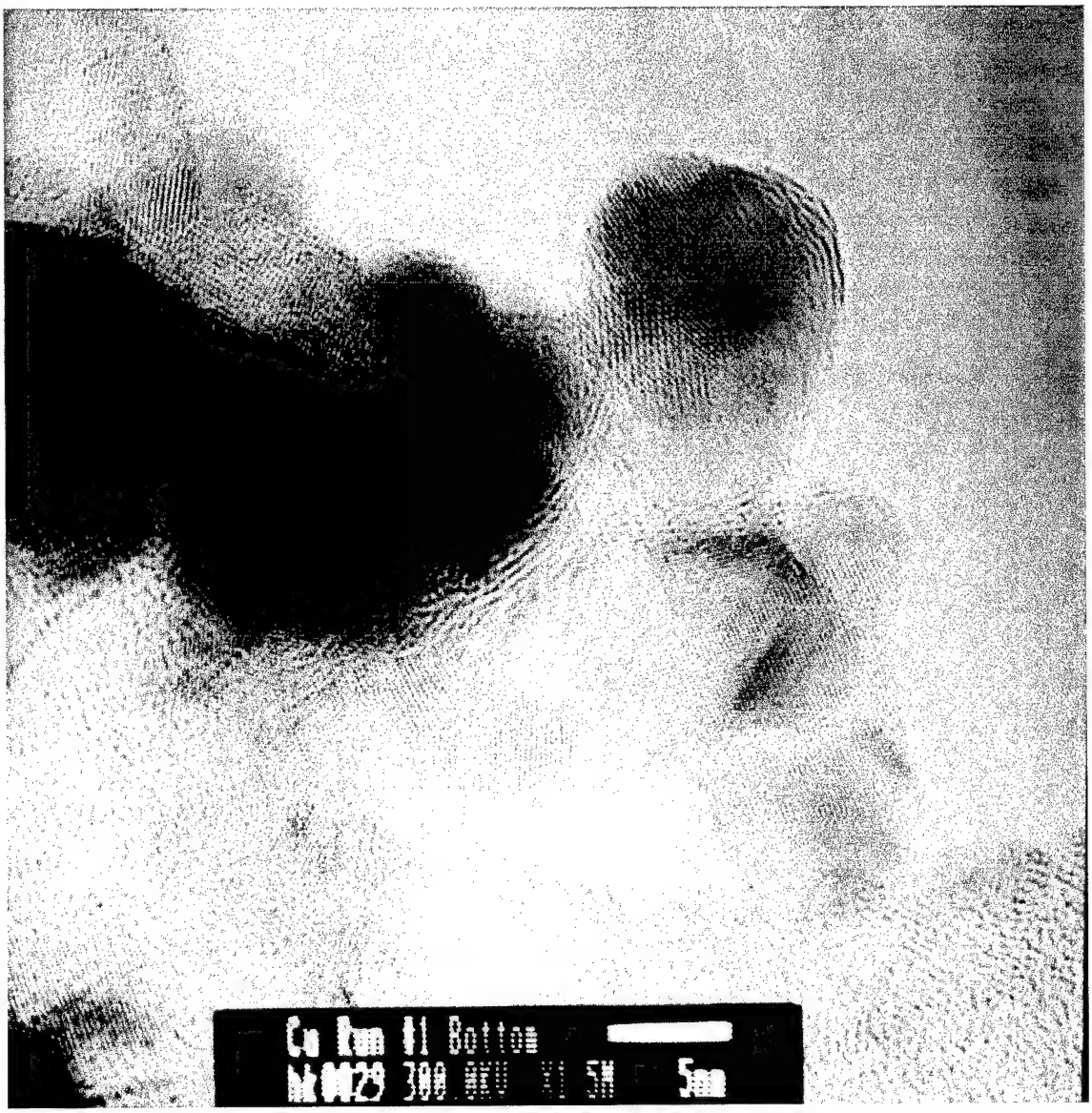

Figure 23. TEM micrograph of copper powder particles. No well-defined passivation layer structure is evident. The white bar length is 5 nm.

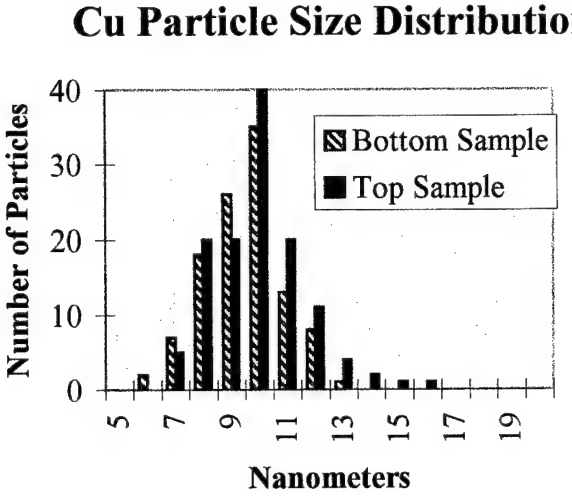

Figure 24. Particle size distributions for copper powders collected from the top and bottom of the collection rod assembly. Average particle size is 10 nm and the distributions have FWHMs of 3 nm.

The absolute purity of the copper powders was determined using Rutherford backscattering spectrometry and high-energy nuclear resonance spectrometry[1]. RBS was used to detect major and minor elemental components that are heavier than helium. Figure 25 shows a typical RBS spectrum that was collected at 2 MeV from a hand-pressed pellet of the nanometer-scale copper powder. The spectrum shows that no contaminant levels exist that are greater than 0.1 atomic percent. Thus, the copper powders are very pure.

Figure 25 also shows no obvious oxygen content in the sample. We expected to have oxygen in the sample due to the passivation process that is integral to our overall fabrication process. Obviously, the passivation process that we use is much less effective for copper than for magnesium. To determine the actual oxygen content, we used a $^{16}O(\alpha,\alpha)^{16}O$ nuclear resonance[2] at 7.6 MeV to enhance our sensitivity to oxygen by a factor of 141 over the kinematic (Rutherford) value. Figure 26 shows the spectrum obtained and reveals that the oxygen content in the copper samples is approximately 2 at. %. We believe that the low oxygen content (and subsequent minimal passivation) in the copper powder is due to the low evaporation temperature of CuO relative to the melting temperature of copper metal. When the copper nano-particles are formed in our deposition apparatus, the temperature of the particles is probably higher than the evaporation temperature for CuO as the particles pass through the passivation section of the apparatus. This would result in minimal passivation-layer formation, which is what we observe for our copper powders. Passivation of nanometer-scale copper powder does not seem to be of any particular practical benefit, as the nanometer-scale copper powder is

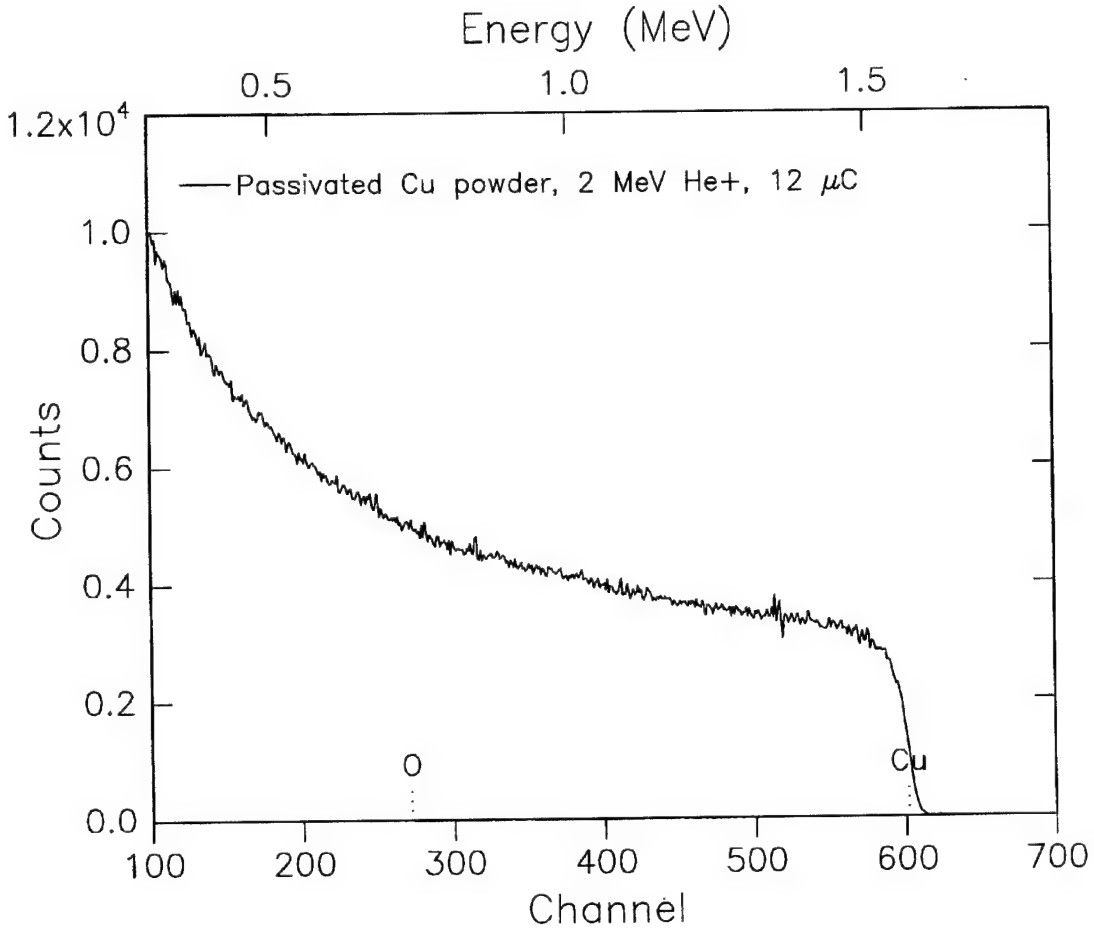

Figure 25. 2-MeV RBS spectrum from a hand-pressed pellet of nanometer-scale copper powder particles. Elemental contaminant levels are below 0.1 atomic percent. Sensitivity of RBS to oxygen in the presence of copper is insufficient to detect it at low (few percent) concentrations. An accurate oxygen concentration measurement for this sample is shown in Fig. 26.

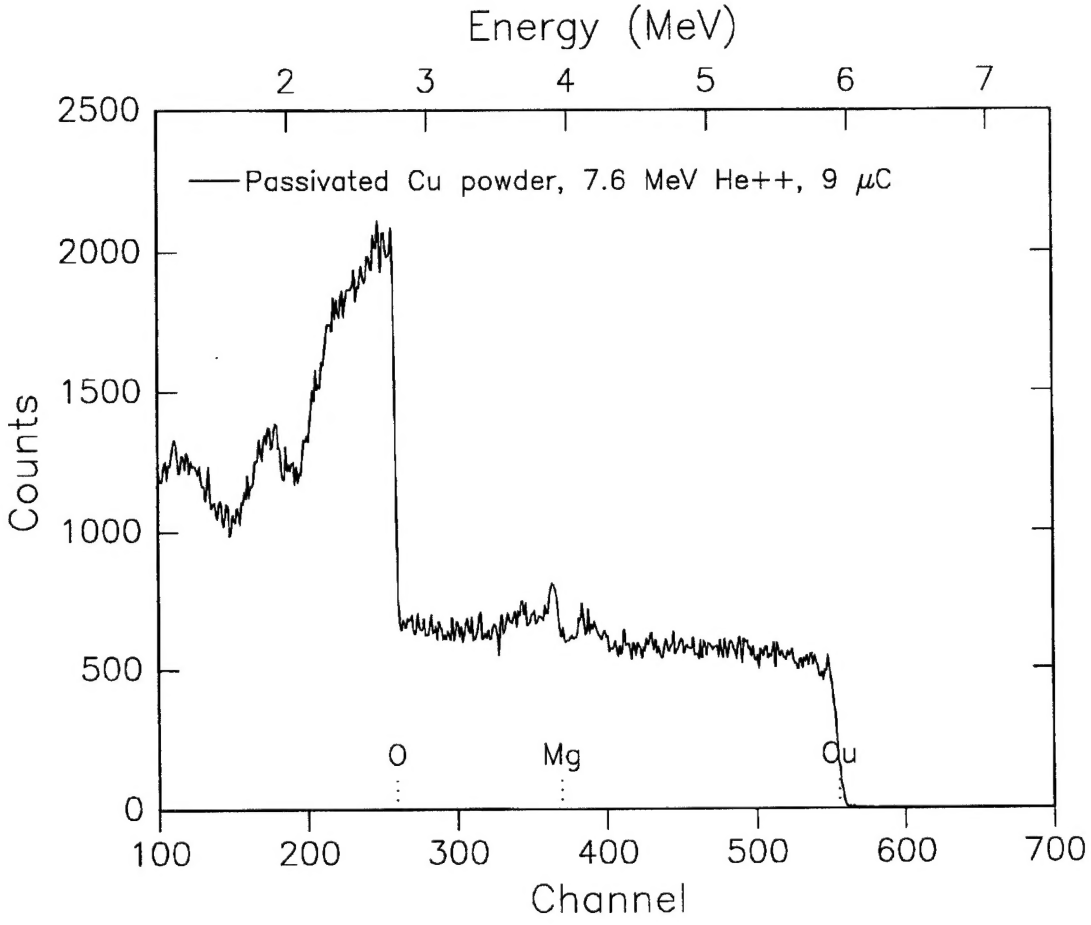

Figure 26. $^{16}O(\alpha,\alpha)^{16}O$ nuclear resonance spectrum at 7.6 MeV from a hand-pressed pellet of nanometer-scale copper powder particles to determine the oxygen concentration. The oxygen sensitivity enhancement factor is 141 for this resonance. The oxygen concentration in the sample is 2 at. %, revealing that minimal passivation by CuO is present on the powder particles. Nevertheless, the nanometer-scale copper powder is not pyrophoric. A small amount (<1 at. %) of magnesium is detected at the surface of the pressed pellet, due to cross contamination that occurred during handling and pressing of the pellet. No magnesium is present in the bulk of the copper powder.

not pyrophoric. It is expected that a CuO passivation layer could be formed (if desired) by modifying the fabrication apparatus to permit additional cooling of the nanometer-scale copper particles before the passivation step is attempted. This could be accomplished by extending the physical path length between the copper evaporation source and the passivation section in the apparatus. Additional path length between the two units would provide additional time for cooling collisions to occur between the carrier gas molecules and the copper particles. At some critical length, the particles would be cool enough to support a stable oxide passivation layer.

Small-scale apparatus design

It is possible to estimate what sample size will be required in a larger-scale apparatus that can produce powder at a rate of 1-2 kg/day by extrapolating data obtained during our laboratory-scale experiments. The pertinent data from our laboratory-scale experiments include measurements of sample size (evaporating area) at the source and powder flux (mass/time) at the collector. The source crucible for our laboratory-scale apparatus is a cylindrical boron-nitride cup of dimensions: ¼"-diameter x 11/16"-long with 1/32"-thick walls. The source crucible is inserted into the outer edge (wall) of a 1"-diameter graphite susceptor with a 1/4"-thick wall. Taking our experimental results for aluminum, the effective flux (amount of powder collected for a fixed deposition period) from the laboratory-scale apparatus is approximately 60 mg per 5 minutes, for a crucible operating temperature of 1600 °C. These parameters correspond to a production rate of :

$$\text{production rate} = \text{flux} / (\text{area of crucible mouth}) / \text{unit time} \sim 25 \text{ g-hr}^{-1}\text{-sq. in.}^{-1}$$

for aluminum powder. If a production day is considered to be an 8-hour period and 2 kg of powder must be produced, then a flux of

$$R = 2 \text{ kg/8-hour day} = 250 \text{ g/hr}$$

is required. The evaporating area required to produce 250 g/hr flux at the current (per-unit-area) production rate is

$$A = (250 \text{ g/hr}) / (25 \text{ g/hr/sq. in.}) = 10 \text{ sq. in.}$$

That area is the same as the area of a disk 3.5" in diameter. Such a disk could be used to achieve the required flux. Alternatively, and more efficiently, one could utilize an annular evaporation surface of equivalent area, instead of the surface of a disk, in order to achieve high coupling efficiency to the induction power supply. This is true because the center of a conductive disk within the field of an rf induction coil receives the least amount heating, whereas the edge receives the highest. That is, heat generation at the center of a conductive disk is minimum because the magnitude of induced rf current in a disk is minimum at the center and maximum at the edges. Therefore, if an annular geometry is used as opposed to a disk shape, more efficient coupling to the rf induction field can be

obtained. If the thickness of the annulus is arbitrarily chosen to be 0.5", then the outside and inside radii can be determined from:

$$A_{annulus} = \pi (r^2_{outside} - r^2_{inside}) = 10 \text{ sq. in.} \quad \text{and} \quad r_{outside} - r_{inside} = 0.5".$$

For this case, $r_{outside} = 3.43"$ and $r_{inside} = 2.93"$. An annular source of these dimensions can be easily contained within the volume of a typical high-temperature stage of a large-scale production apparatus. The annular area calculated above will produce the flux required to produce 2 kg of powdered aluminum in a single 8-hour day, providing that the annular evaporating surface is maintained. The annulus can be the top surface of a cylinder of molten aluminum that is steadily evaporating away or the top surface of an annular ring of molten aluminum that is continually being replenished from an internal or external source as quickly as aluminum evaporates. Either geometry is acceptable, in principle. An annular cylinder with $r_{outside} = 3.43"$ and $r_{inside} = 2.93"$ that contains 2 kg of aluminum (2.7 g/cc density) would have a height of

$$h = \text{annular volume / annular area} = 4.5 ".$$

This dimension is also compatible with the volume available in a typical large-scale apparatus. The above calculations serve to demonstrate that scale up of our current powder production process to the 2 kg/day level is not at all unreasonable. In fact, the argument suggests that our proposed effort is quite feasible, at least from a flux rate and evaporation area viewpoint.

The power that will be required for a small-scale apparatus can be estimated from the results of our laboratory-scale apparatus. In the laboratory-scale demonstrations, maximum power was used to fabricate the aluminum nano-powder; i.e., 2.5 kW. To first order, the power required for the small-scale apparatus will scale proportionally with the increase in surface area that is heated to the operating temperature, as no change in operating temperature is desired. Thus, the power required for the small-scale apparatus is estimated to be

$$P = 2.5 \text{ kW} \times \text{required surface area/present area of graphite susceptor}$$

$$= 2.5 \text{ kW} \times (10 \text{ sq. in.} / \pi (0.5^2 - 0.25^2 \text{ sq. in.})) = 42 \text{ kW}.$$

This power level is readily obtainable using off-the-shelf rf induction power supplies at moderate cost. The above power estimate assumes that the depth of heated material is similar between the laboratory-scale apparatus and the small-scale apparatus, i.e., nominally 11/16" thick. The assumption is true for a small-scale apparatus that employs a raw-material feed capability as opposed to a batch-mode of operation. Higher power levels will be required for a batch-mode unit as compared with a continuous-feed-mode unit, as batch-mode operation requires a larger mass to be heated to the operating temperature.

Some optimization in power efficiency can likely be realized by selecting an optimum operating frequency. This optimization is accomplished by matching the effective sample size with the intrinsic field penetration depth. However, a calculation of the optimal frequency requires precise knowledge of the resistivity of the metal at the operating temperature. This value will vary depending upon the metal being used. In practice, a useful rule of thumb for heating metals is to operate at a sufficiently high frequency that the penetration depth is much smaller than the sample size. As long as the thermal conductivity of the sample is reasonably high, as is nearly always the case with metals, operation at high frequencies (i.e., a few hundred kilohertz) results in good efficiency.

Based upon the above considerations, our design for a small-scale apparatus capable of producing 1-2 kg/day of nanometer-scale metal requires at least a 100 kW radio frequency induction power supply that operates near 200 kHz. The high-temperature stage would need to have a minimum diameter of 6 inches, to be able to house a crucible that has a 10 sq. in. evaporation surface. A method of continuous raw material feed (coarse powder feed) will be required to maintain reasonable efficiency. In addition, gas re-circulation equipment will be required. Otherwise, the cost of helium for an all-day operation will be prohibitively expensive. The physical design of the small-scale apparatus is not substantively different from that shown in Fig. 2. As such, the plan for construction for the small-scale apparatus is that outlined in our Phase I proposal for the laboratory-scale apparatus, with appropriate allowances made for increased time for construction and testing of a continuous-feed mechanism and gas circulating equipment. Additional time and expense must also be allowed for installation of larger-scale utilities that will be required, especially services for increased electrical power and increased cooling water capacity.

Conclusion

The principal conclusion for this Phase I feasibility study is that dynamic gas condensation is a viable technique for the commercial production of high-purity, nanometer-scale metal powders. The powders that were produced in this study have no equivalent in the current commercial sector. Competing technologies, such as exploding wire techniques and plasma-based techniques, simply do not produce powders with such small particle diameters, such narrow size distributions, or such high purity. Engineering considerations and estimates relating to scale up of the dynamic gas condensation technology reveal no insurmountable problems. Our conclusion is that dynamic gas condensation is a feasible technique for continued development in large-scale, nanometer-scale metal powder production.

Acknowledgment

We gratefully acknowledge the use of the User Facility Program, the Limited Term Use of Laboratory Property Program, and the Small Business Technical Assistance Program at Los Alamos National Laboratory.

References

1. Handbook of Modern Ion Beam Materials Analysis, eds. Joseph R. Tesmer, Michael Nastasi (Materials Research Society, Pittsburgh, Pennsylvania, 1995).
2. *ibid.*, p. 501.